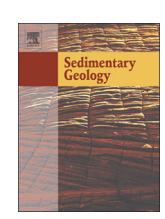
FISEVIER

Contents lists available at ScienceDirect

Sedimentary Geology

journal homepage: www.elsevier.com/locate/sedgeo



Constraining the timing, kinematics and cyclicity of Mississippian-Early Pennsylvanian glaciations in the Paraná Basin, Brazil



Eduardo L.M. Rosa ^a, Fernando F. Vesely ^a, John L. Isbell ^b, Felipe Kipper ^c, Nicholas D. Fedorchuk ^b, Paulo A. Souza ^c

- ^a Departamento de Geologia, Universidade Federal do Paraná, Caixa postal 19001, CEP 81531-980 Curitiba, PR, Brazil
- ^b Department of Geosciences, University of Wisconsin-Milwaukee, Milwaukee, WI 53211, USA
- C Departamento de Paleontologia e Estratigrafia, Instituto de Geociências, Universidade Federal do Rio Grande do Sul, Caixa Postal 15001, CEP 91501-970 Porto Alegre, RS, Brazil

ARTICLE INFO

Article history:
Received 4 December 2018
Received in revised form 1 March 2019
Accepted 3 March 2019
Available online 06 March 2019

Editor: Dr. J. Knight

Keywords: Late Paleozoic Ice Age Itararé Group Glacial paleogeography Glaciotectonics Subglacial Mississippian

ABSTRACT

Ice-contact deposits emplaced by Late Paleozoic Ice Age (LPIA) glaciers are rarely exposed due to a low degree of preservation and their capping by thick glaciomarine deglaciation sequences. In this paper, we present new data on glacial cyclicity, relative age constraints and paleoice flow interpretations for an ice-contact succession of the lowermost Itararé Group in eastern Paraná Basin (Brazil). The 80 m-thick ice-contact complex rests over the Itararé Group basal unconformity and comprises four stacked informal stratigraphic units regarded as the depositional/ deformational record of three ice lobes advance/retreat cycles. Glacial cycle 1 comprises a sheet of massive diamictite resting on striated pavements carved on Devonian sandstones and topped by grooved/fluted surfaces, which indicate subglacial emplacement from a northward flowing ice lobe. The glacial cycle 2 succession was deposited in a proglacial to ice-marginal marine setting and subsequently deformed due to minor ice margin fluctuations of a westward/southwestward flowing grounded ice lobe. Glacial cycle 3 is interpreted as a thick overridden push moraine composed of grounding-line fan deposits capped by a subglacial diamictite emplaced by grounded ice advancing northwestward. A middle Visean-early Serpukhovian palynomorph assemblage was recorded in cycle two deposits, representing the oldest late Paleozoic glacial rocks in the Paraná Basin. The icecontact complex elucidates multiple waxing and waning phases of the Windhoek Ice Sheet onto the eastern margin of the Paraná Basin during the Mississippian-Early Pennsylvanian, demonstrating that ice sheets of the early stages of the LPIA were also present in the Brazilian-African domain of southwestern Gondwana.

© 2019 Elsevier B.V. All rights reserved.

1. Introduction

Former glaciations are documented in the stratigraphic record by erosional, depositional, and deformational products formed directly or indirectly by glaciers (Frakes, 1979; Crowell, 1999). The Late Paleozoic Ice Age (LPIA) is one of the best understood pre-Cenozoic icehouse intervals and its sedimentary record is widespread in former mid-to-high-paleolatitude sedimentary basins of Gondwana (e.g., Santos et al., 1996; Isbell et al., 2003; Fielding et al., 2008; Limarino et al., 2014).

Nevertheless, the LPIA record is mostly composed of glacially-influenced marine deposits whereas products generated directly by glaciers are rarely recognized in the stratigraphic record (e.g., Almeida, 1948; Starck et al., 1993; Le Heron, 2017). Subglacial erosive landforms located on the basal unconformity of LPIA deposits are the most reliable and widely used structures for reconstructing the kinematics and paleoglaciologic aspects of LPIA glaciers (e.g., Visser, 1987; Bussert,

E-mail addresses: vesely@ufpr.br (F.F. Vesely), jisbell@uwm.edu (J.L. Isbell), fedorch2@uwm.edu (N.D. Fedorchuk), paulo.alves.souza@ufrgs.br (P.A. Souza).

2010; Rosa et al., 2016). Furthermore, glaciotectonic structures, even if rarely described and discreetly used in the LPIA record (e.g., Isbell, 2010; Henry et al., 2012), are also a powerful tool for determining former glacier kinematics (Berthelsen, 1978; Hart and Watts, 1997; Boulton et al., 1999).

The intracratonic Paraná Basin of southwestern Gondwana comprises one of the thickest (up to 1300 m) LPIA records. Glacial deposits are found within the Itararé Group and its time-equivalent units located in other sectors of the basin (Aquidauana, Coronel Oviedo and Aquidabán formations; Rocha-Campos and Santos, 1981; Fúlfaro, 1996). Since the bulk of the Itararé Group is comprised of marine and transitional sequences interpreted as the records of major deglacial cycles (e.g., França and Potter, 1988; Vesely and Assine, 2006), most research has been concerned with characterizing its stratigraphy based on traditional sequence stratigraphy. In this way, glacial extent and cyclicity can only be inferred indirectly from stacking patterns and key surfaces (e.g., Valdez et al., 2017; Vesely et al., 2018). Only at rare isolated localities can thin intervals of subglacial and ice-contact facies be documented on the Itararé Group basal unconformity (e.g., Tomazelli and Soliani, 1997; Vesely et al., 2015).

Ice dynamics in the Itararé Group have primarily been determined by subglacial striations and grooves that show ice flow patterns towards the north and northwest (Rosa et al., 2016; Fallgatter and Paim, 2017). However, in between Itararé Group deposits, glacier kinematics are inferred indirectly from paleocurrent trends in ice-distal facies (e.g., Carvalho and Vesely, 2016; Mottin et al., 2018), and directly by rare layers containing subglacial deformational structures (i.e., Rocha-Campos et al., 2000; Aquino et al., 2016).

The depositional age of the Itararé Group is traditionally defined as late Bashkirian-early Sakmarian based on palynostratigraphy and other fossil groups (Souza, 2006; Holz et al., 2010). Recent U—Pb radiometric dating of interbedded ash-fall deposits has better constrained the timing of the final deglaciation in southern and southeastern Paraná Basin to the Late Pennsylvanian (Cagliari et al., 2016; Griffis et al., 2018a). However, basal ages reflecting the onset of glaciation still remain undetermined.

Among previously reported localities containing ice-contact deposits, the study succession, located in southeastern Paraná State (Balsa Nova region; Bigarella et al., 1967; Trosdtorf et al., 2005; Vesely et al., 2015), is remarkable because it is relatively thick (several tens of meters) and contains a rich archive of glaciogenic deposits and structures (Fig. 1). In order to evaluate the significance of the ice-contact succession to the paleogeographic and paleoenvironmental setting in the eastern margin of Paraná Basin and contiguous regions in southwestern Africa during the early stages of the LPIA, the main aims of this work are: (i) to define a detailed glacial cyclicity based on reconstruction of former depositional environments; (ii) to determine local paleoice flow directions using glaciotectonic, erosional, and depositional structures; (iii) to determine relative depositional age by biostratigraphy; and (iv) to constrain the timing of glacial advances.

2. Geological setting

The studied ice-contact complex is exposed on the eastern margin of the Paraná Basin around the localities of Balsa Nova, São Luiz do Purunã, and Witmarsum, southeast Paraná State (Fig. 2). Locally, the strata are equivalent to the basal portion of the Itararé Group (Lagoa Azul Formation) named as units "1-A" and "1-B" by Vesely et al. (2015) (Fig. 1). The ice-contact deposits rest on a gently angular unconformity cut on Lower Devonian sandstones of the Furnas Formation. In the central and northern portions of the study area, the succession rests over Precambrian phyllites. The ice-contact succession is capped by glacially-influenced proglacial subaqueous fan and deltaic deposits defined as "unit 2" by Vesely et al. (2015).

The presence of glaciogenic features in this area has long been reported, including striated surfaces on the Devonian substrate and subglacial tillites, as well as soft-sediment deformation attributed to ice squeeze (Fuck, 1966; Muratori, 1966; Bigarella et al., 1967; Trosdtorf et al., 2005; Canuto et al., 2010). Vesely et al. (2015) proposed that the deposition of the ice-contact succession was controlled by an unconfined, fluctuating terrestrial ice margin that advanced towards the north and northwest during two separate advance/retreat glacial cycles. They interpreted the associated facies as subglacial tillites (unit 1-A) and glaciotectonized lacustrine outwash (unit 1-B). The exact age of these deposits is poorly defined because of the absence of fossiliferous horizons and any syndepositional volcanic ash layers. An age not younger than the Moscovian/Kasimovian boundary was indicated by palynomorphs recovered from glaciomarine rhythmites of unit 3 located ~60 m above the ice-contact complex (Kipper et al., 2017) (Fig. 1).

3. Methods

This research was conducted through field examination of sedimentary facies, exhumed erosive landforms, and penecontemporaneous soft-sediment deformational structures from a total of 47 outcrops around the localities of Balsa Nova, Witmarsum, and São Luiz do Purunã.

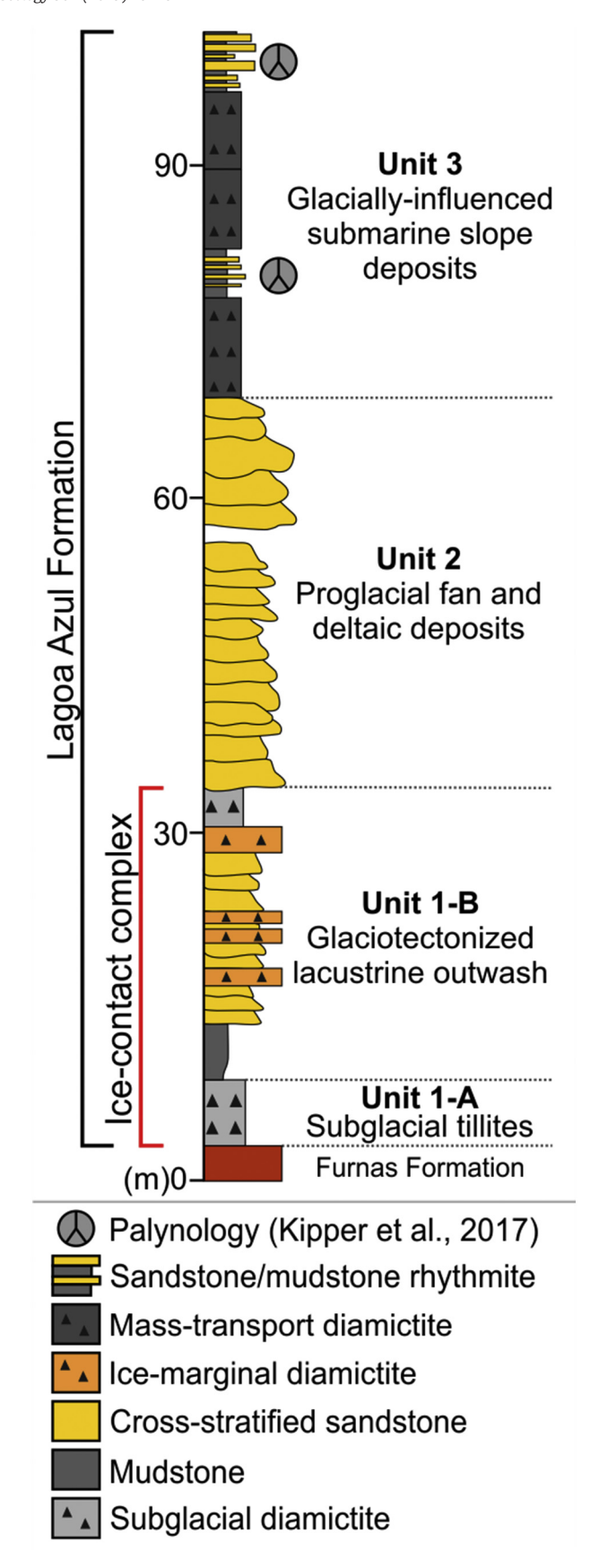


Fig. 1. Composite stratigraphic section adapted from Vesely et al. (2015) of the Lagoa Azul Formation in southeastern Paraná state with individualized informal units and their respective interpreted depositional environments. The ice-contact complex analyzed in this study comprises units 1-A and 1-B.

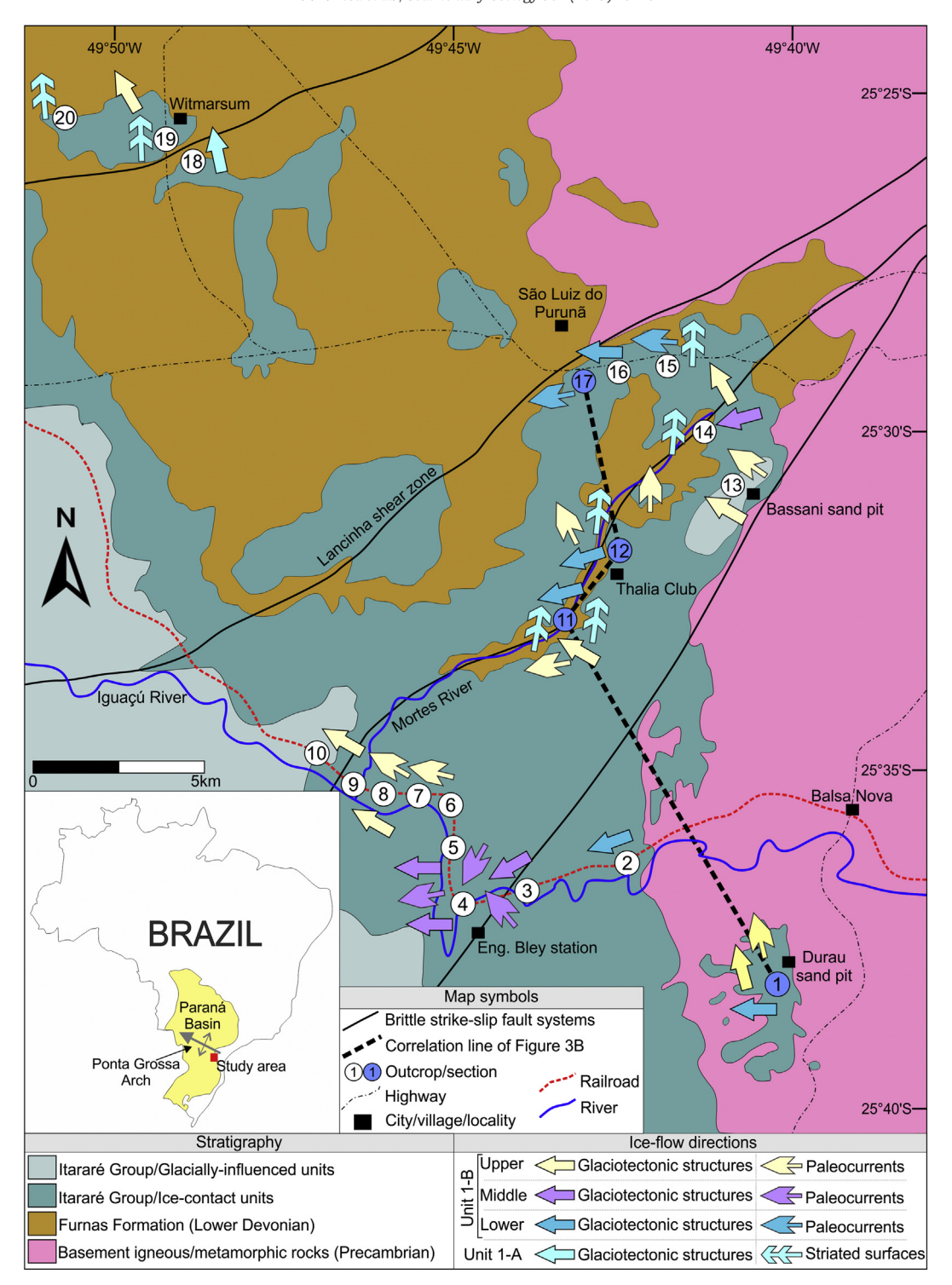


Fig. 2. Geological map of the study area with the indication of main outcrop localities and ice flow directions obtained from subglacial striated surfaces, glaciotectonic structures and paleocurrents.

The lithotype classification scheme of Hambrey and Glasser (2012) was followed due to the abundance of poorly-sorted lithotypes. Five vertical stratigraphic sections were measured at 1:50 scale containing a total of ~236 m of strata. Among these, a composite stratigraphic section ~85 m thick, comprising all units discussed in the text, was generated from outcrops located along a railroad track (localities 2 to 10; Fig. 2).

Palynological analysis was performed in samples retrieved from laminated heterolithic (sample BN-1) and muddy, fine-grained sandstone facies (sample BN-2) (Fig. 3A). Palynological sample processing followed the standard methods for Paleozoic material. Carbonates and

silicates were removed using HCl and HF, respectively; palynomorphs between 20 and 250 μm were concentrated by sieving; glass slides were prepared from few drops of residue mounted with polyester resins, which are housed in the Paleontological Museum of the Universidade Federal do Rio Grande do Sul, under codes MP-P 13796, 13797, 13798, and 13799. Taxonomic assignments were made under optical light microscopy by means of comparison with species described in the literature.

In order to characterize glacier kinematics, 1193 measurements of deformational structures interpreted to be of glaciotectonic origin,

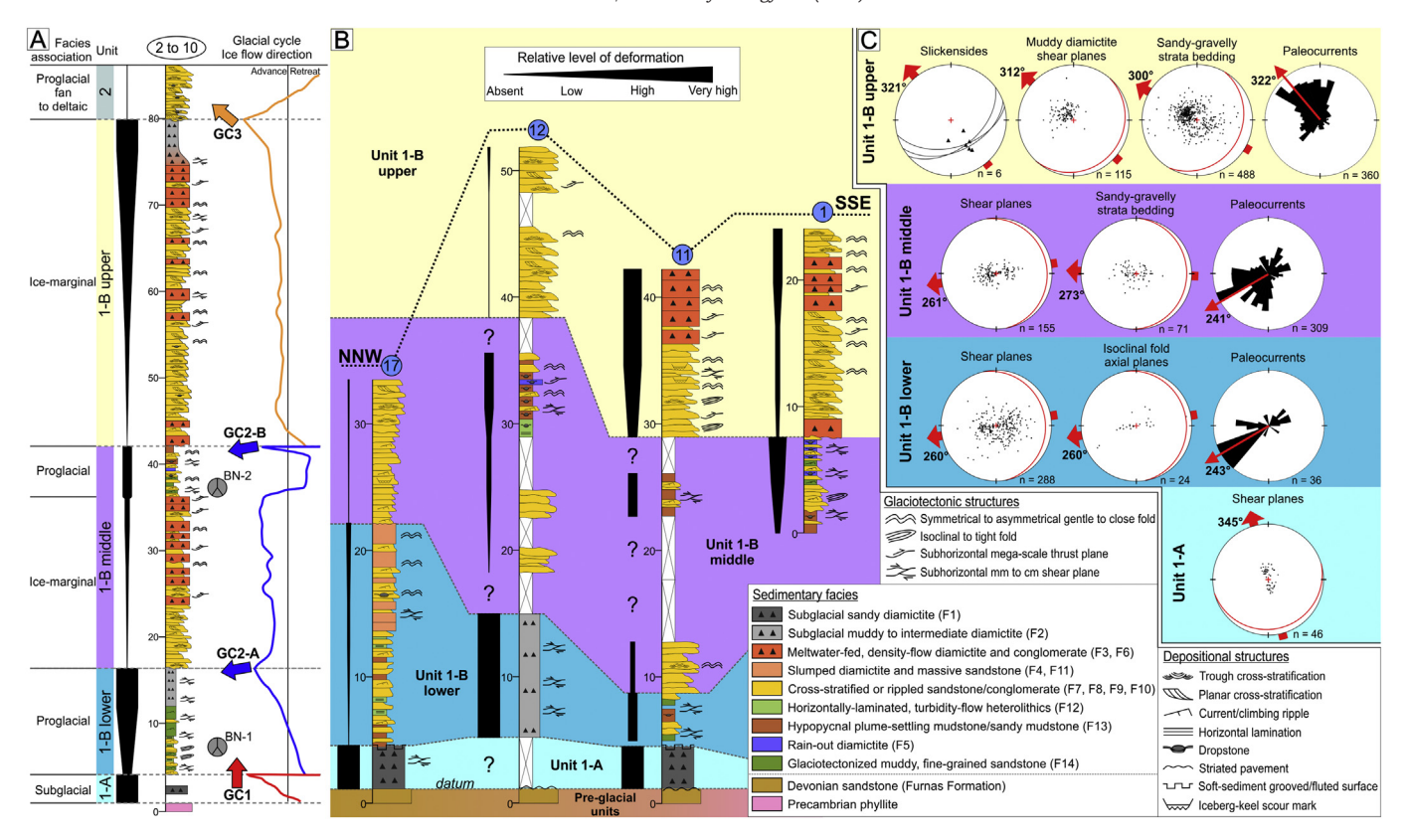


Fig. 3. (A) Composite stratigraphic section constructed from outcrops along the railroad track in the study area (localities 2 to 10) showing individualized units, unconformities (gray dashed lines), relative level of deformation, facies associations, interpreted glacial cycles (GC) with paleoice flow directions, and palynologic-sampled intervals; (B) North/northwest-south/southeast correlation of sections located in Fig. 2 and architectural framework of the defined units. Inferred degree of deformation shown by black bars next to each section; (C) Pole-to-plane stereographic projections of soft-sediment deformational structures and synoptic rose diagrams with paleocurrent data for each unit. (For interpretation of the references to color in this figure legend, the reader is referred to the web version of this article.)

such as mm- to m-scale shear planes/surfaces, folded bedding, and slickensides were collected and analyzed in pole-to-plane equal-area stereographic projections. The paleoice flow was inferred from the upglacier dip direction of these structures (e.g., van der Wateren, 2002; Phillips, 2018). Seven bedrock and intraformational subglacial striated/grooved surfaces were also measured, five of them reported here for the first time. In addition, 705 paleocurrent measurements were collected from current- and climbing-rippled sandstones, cross-stratified sandstones and conglomerates.

4. Stratigraphic framework

The combined analysis of sedimentary facies, stacking patterns, deformational styles and the orientation of glacier kineto-indicators were used to define four informal stratigraphic units (Fig. 3). These are unit 1-A as previously defined by Vesely et al. (2015) and three units equivalent to unit 1-B of the same authors, termed here as 1-B lower, 1-B middle and 1-B upper (Figs. 1, 3A). Such units compose an up to 80 m-thick vertical profile that is significantly thicker than the previously described 35 m-thick section.

The facies and their interpreted depositional/deformational formative processes are shown in Table 1. Most facies are, to some extent, modified by subsequent deformation. All stratigraphic boundaries are marked by erosive surfaces and abrupt changes in the deformation intensities (Fig. 3A, B). Kineto-indicators are presented for each unit using stereographic projections of soft-sediment deformational glaciogenic structures and synoptic rose diagrams with paleocurrent measurements (Fig. 3C).

4.1. Unit 1-A and basal unconformity

The unconformity that underlies the studied succession is defined by at least five striated pavements carved on Devonian sandstones which are placed at different locations throughout the study area. No similar surfaces were found over Precambrian metamorphic rocks. These pavements are flat, have an area of up to 2500 m², comprise straight and parallel shallow grooves, ridges, and striations with a north-south mean orientation. At Witmarsum (locality 19), the grooves and striations occur on the surface firstly documented by Bigarella et al. (1967) and exhibit a 358° orientation. Another striated pavement, described here for the first time, occurs at locality 20 and displays a mean orientation of 355° (Fig. 4A). Additionally, three first-time reported pavements located along the margins of the Mortes River (localities 11, 12, and 14) consist of shallow grooves and striations oriented between 6° to 10° (Fig. 4B-D). At one of these surfaces (locality 12; Thalia Club), several crescentic gouges up to 15 cm-wide indicate a northward paleoice flow (Fig. 4C).

Sandy, clast-poor, massive diamictites up to 7 m thick (F1) are discontinuously exposed overlying the basal unconformity. The diamictites are non-stratified, but their matrix shows cm-thick, anastomosing subhorizontal shear planes (Fig. 4E) with a mean dip direction towards the southeast and an applied stress/ice flow direction towards the northwest (345° mean azimuth; Fig. 3C). Clasts are mainly subrounded, pebble to cobble sized, and have facet and bullet shapes. The upper boundary of the diamictites is characterized by a laterally extensive flat surface with grooves, ridges and flutes. Trosdtorf et al. (2005) previously described a surface at locality 15 with asymmetric small flutes, indicating a northward direction of ice flow (2° mean azimuth).

Table 1Described sedimentary facies with respect of its depositional and deformational aspects.

F	Lithology	Depositional and deformational structures	Formative processes
F1	Sandy, clast-poor diamictite comprising faceted and bullet-shaped clasts ranging from granule to cobble size	Massive, with subhorizontal cm-spaced anastomosing shear planes. Floored by striated pavements and topped by intraformational soft-sediment surfaces containing grooves, flutes and ridges	Debris accumulation and homogenisation by simple shear below an advancing glacier on bedrock (i.e., basal deforming layer)
F2	Homogeneous, muddy to intermediate, clast-poor diamictite with striated, bullet-shaped and faceted clasts ranging from granule to cobble	Massive and showing subhorizontal mm- to cm-spaced shear planes. Clasts are oriented parallel to shear trend. Locally displays slickensided contact with other facies	Simple shear deformation and homogenisation imposed by an advancing glacier over non-consolidated sediments
F3	Polymictic, sandy, clast-rich diamictite with rounded to faceted clasts up to boulders	Arranged in tabular strata up to 2 m-thick; internally massive with incipient long-axis clast orientation. Sometimes floored by concave-up surfaces. Commonly grades to massive and current-rippled sandstones	Deposition from concentrated to hyperconcentrated meltwater flows emanated from tunnels at the glacier margin. Indicative of high meltwater discharge
F4	Sandy to intermediate, clast-poor diamictite with heterogeneous to homogeneous matrix and clasts ranging from granules to pebbles	Tabular beds up to 1 m-thick with relicts of current ripples displaced by several small normal faults	Resedimentation by slumps in a subaqueous setting
F5	Sandy to intermediate, clast-rich diamictite with granule- to cobble-sized clasts	Massive to faintly-stratified. Internal faint stratification defined by mudstone laminae	Association between ice-rafted debris rain-out and settling of hypopycnal plumes
F6	Polymictic conglomerate with clasts up to boulders in a sandy matrix	Massive, with an irregular basal contact containing flame structures; m-scale mudstone rip-up clasts at the base	Deposition from subaqueous hyperconcentrated and highly erosive flows close to the glacier margin. Indicative of water-saturated sediments and rapid sedimentation
F7	Oligomictic conglomerate with sandy matrix	Mid-scale planar and trough cross-stratification. Foresets often grade downflow to gravelly sandstones	Dune migration under high-energy bedload-dominated flows
F8	Medium-grained to gravelly sandstone. Clasts up to boulders occur dispersed	Tabular and concave-up strata with low- to medium-angle planar and trough cross-stratification	Dune migration under high-energy bedload-dominated flows combined with minor deposition from ice-rafted debris rain-out
F9	Well-sorted, muddy to medium-grained sandstone containing outsized clasts up to cobbles	Sinuous crested current ripples	Migration of subaqueous ripples under lower flow regime conditions and coeval ice-rafted debris rain-out
F10	Well-sorted, fine-grained sandstone. Locally displays rare outsized clasts up to pebble size	Sets up to 5 cm comprising climbing ripples	Deposition from turbidity flows plus minor ice-rafted debris rain-out and hypopycnal plume settling
F11		Massive; often grades upwards to current-rippled sandstones	Concentrated density flow triggered by gravity and/or meltwater input in a subaqueous setting
F12	Heterolithic facies defined by an alternation of fine-grained sandstone and mudstone laminae	Rhythmic laminae (mm- to cm-thick) displaying normal grading between mudstone/sandstone pairs. Laminae sets are fairly truncated. Locally, sandy laminae occasionally have small current ripples and muddy laminae are thicker. Outsized clasts pierce the lamination	Deposition from a combination of turbidity flows, ice-rafted debris rain-out and settling of hypopycnal plumes
F13	Mudstone to sandy mudstone with dispersed clasts up to cobbles	Massive	Fast mud settling from hypopycnal plumes associated with minor ice-rafted debris rain-out
F14	Muddy, fine-grained sandstone with bullet- shaped and faceted clasts up to cobble size	Massive and heterogeneous matrix with remnants of current and climbing ripples and horizontal lamination. Pervasive subhorizontal mm- to cm-spaced shear planes. Stretched out mudstone clasts. Outsized clasts deform the remnants of stratification	Glaciotectonic deformation of low-energy subaqueous facies (F9, F10, F12, F13) imposed by subglacial and ice-marginal shear during a glacier advance

A new surface at locality 11 has parallel deep grooves and ridges trending 8°-188° but with no clear indicators of ice flow direction (Fig. 4F).

4.2. Unit 1-B lower

Unit 1-B lower is up to 18 m thick and is highly variable in terms of composition and deformational structures (Fig. 3A, B). In a predeformational context, it is composed of two facies associations that exhibit a general coarsening-upward trend. At the base, there is an association dominated by fine-grained facies (Fig. 5A-C). This association includes intercalations of current- and climbing-rippled sandstones (F9, F10) associated with laminated heterolithics (F12), and massive, sandy mudstones with dispersed outsized clasts (F13). Above the fine-grained association, a sandy succession is locally observed (Fig. 5D), consisting of intercalated beds of current-rippled sandstones (F9), heterogeneous clast-poor diamictites often containing internal diffuse bodies of current-rippled sandstones displaced by cm-scale normal faults (F4; Fig. 5E), and massive sandstones (F11). Throughout the entire unit, paleocurrents from non-deformed current-rippled sandstones show a southwestward trend (243° mean azimuth; Fig. 3C).

The pattern of deformation across different localities is highly variable, ranging from non-deformed to highly-deformed facies. At locality 2, a railroad cut contains a 10 m-high succession with a distinct

upward variation in deformation patterns and degree of homogenisation (Fig. 6A-E). The original beds of rippled sandstones and heterolithics dominate in the lower portion of the exposure and contain rootless isoclinal folds with subhorizontal axial planes verging westward/southwestward (260° mean azimuth; Fig. 3C). In the middle portion, these sandy layers become more boudinaged and disrupted (Fig. 6A) before disappearing entirely in the upper portion.

Muddy, fine-grained sandstones with both a massive and heterogeneous matrix contain relicts of ripples and horizontal laminations as well as stretched mud clasts and outsized clasts (F14; Fig. 6B-D). This facies appears in the lower portion of the exposure between the folded layers and dominate in the middle portion. The upper portion of the exposure is characterized by massive, homogeneous, intermediate, sheared diamictites (F2; Fig. 6E). Mm- to cm-scale, subhorizontal, anastomosing shear planes highlighted by oxides occur throughout the exposure but are more abundant in the middle and upper portions. In the sandy strata at the bottom of the unit, the original depositional structures are often dislocated by several fractures dipping to the east.

Locality 12 exhibits an 8 m high exposure of intermediate, clast-poor diamictite with a homogeneous matrix and no preserved depositional structures (F2). The diamictite is cut by several subhorizontal, anastomosing, cm-scale shear surfaces highlighted by oxide infiltration. A few disrupted bodies of sandstones occur dispersed throughout the exposure. The sandy-muddy character of the diamictite matrix, the

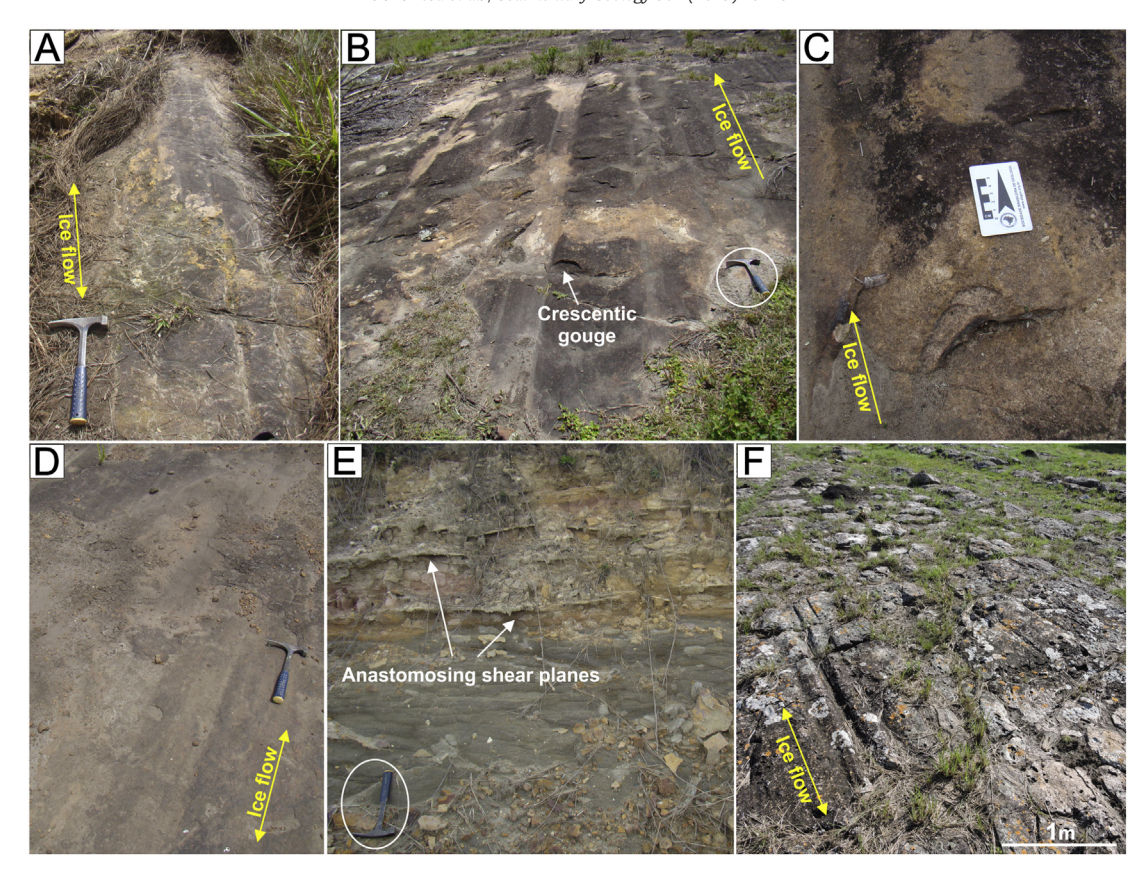


Fig. 4. Main facies and erosive features related to unit 1-A. (A) Striated surface on Devonian Furnas sandstones at Witmarsum (locality 20); (B) flat grooved/striated surface on Devonian Furnas sandstones at Thalia Club (locality 12) containing (C) crescentic gouges; (D) shallow striation over Furnas sandstones near Mortes River (locality 11); (E) massive, clast-poor, sandy diamictite (F1) with subhorizontal anastomosing shear surfaces; (F) flat soft-sediment subglacial surface near Mortes River (locality 11) developed on top of diamictites.

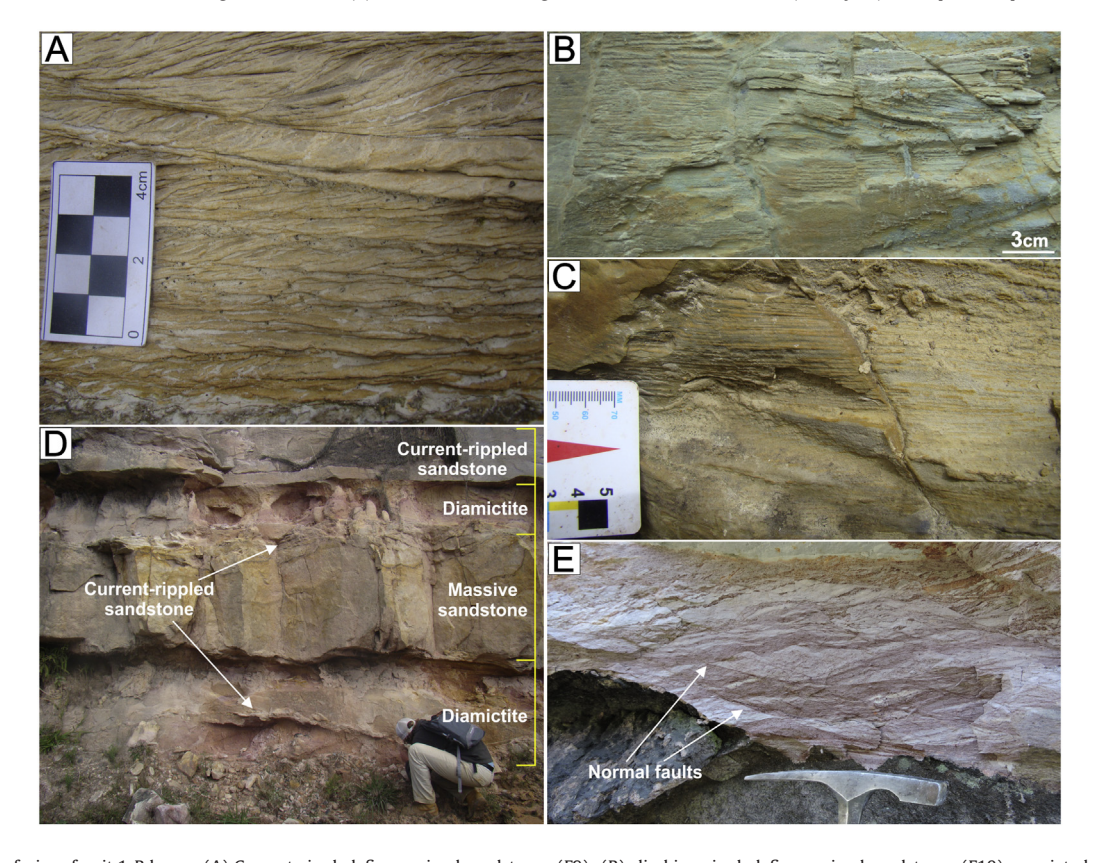


Fig. 5. Sedimentary facies of unit 1-B lower. (A) Current-rippled, fine-grained sandstones (F9); (B) climbing-rippled, fine-grained sandstones (F10) associated with (C) laminated heterolithics with mm-thick, fine-grained sandstone/mudstone pair (F12); (D) gently-deformed intercalation between current-rippled (F9) and massive (F11) sandstones with interbeds of clast-poor, sandy to intermediate diamictites (F4); (E) detail of F4 diamictite matrix with relicts of current-rippled sandstones dislocated by small normal faults.

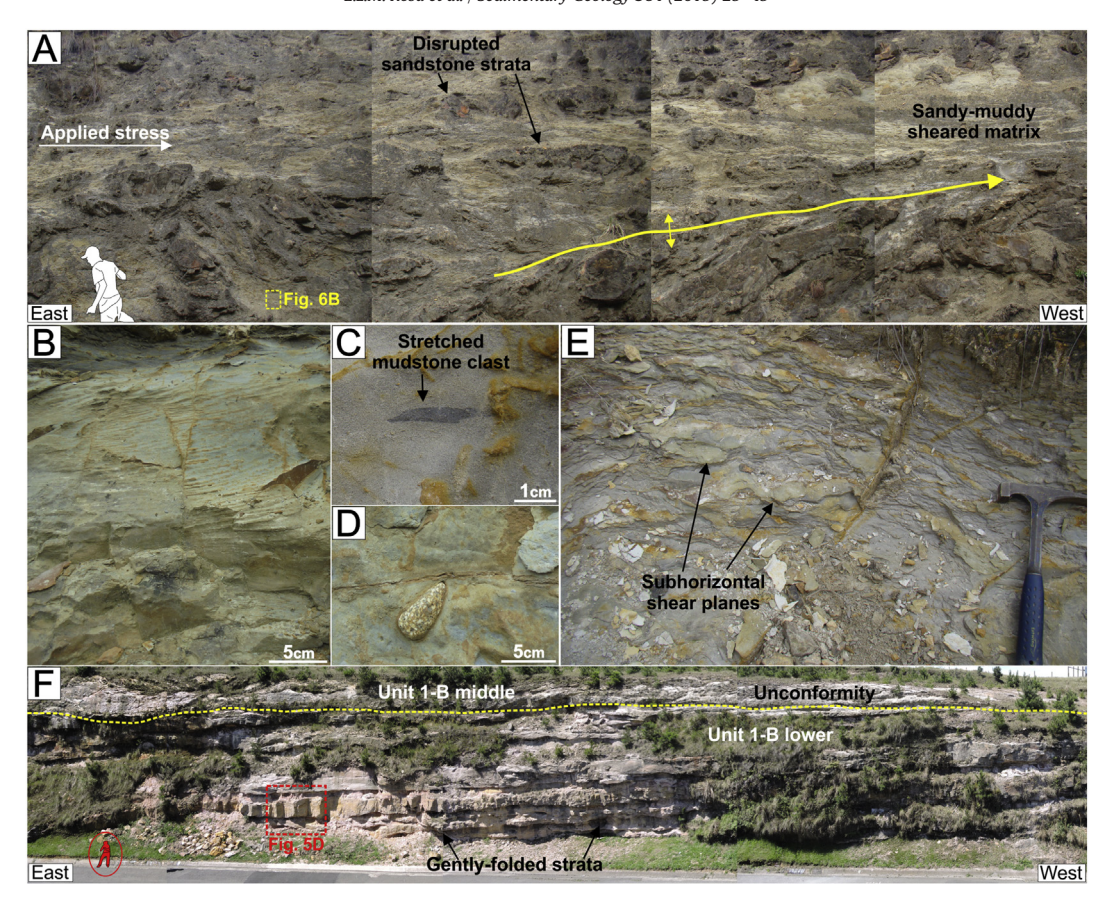


Fig. 6. Main deformational structures and patterns of unit 1-B lower. (A) Lower and middle interval of a railroad cut exposure (locality 2) with deformed strata disposed in isoclinal folds at the base and more disrupted towards the top; (B-D) muddy, fine-grained sandstones containing relicts of depositional structures, stretched mudstone clasts and dispersed outsized exotic clasts (F14); (E) sheared intermediate diamictite (F2) disposed at the top of the railroad cut; (F) gently-folded top layers of the sandy association of unit 1-B lower at locality 17 below a major truncation erosive surface (yellow dashed line) overlain by non-deformed basal sandstones of unit 1-B middle. (For interpretation of the references to color in this figure legend, the reader is referred to the web version of this article.)

similarity of the deformational structures, and its stratigraphic position place this outcrop at the same level as the upper portion of locality 2, where the sheared diamictite sits on folded heterogeneous strata. The low-angle shear surfaces from throughout the fine-grained facies of unit 1-B lower are undulating and their orientation show a moderate degree of dispersion (Fig. 3C). Despite that, the stereographically-calculated mean plan resulted in a dip towards the east/northeast (N80/10) and a structural vergence to the west/southwest (260°).

At the top of unit 1-B lower, a sandy facies association outcrops locally and its original bedding is better preserved than the fine-grained association from the lower portion. At locality 16, the strata are disposed in slightly asymmetric open and close large folds. The exposure at locality 17 (Fig. 6F), approximately 2 km west of locality 16, displays slightly deformed tabular strata. Such strata are tilted at low angles to the east, exhibiting gentle symmetrical folds and thinned/thickened layers (Fig. 5D). Some reverse faults dipping to the east also occur, however, normal faults dipping both towards the east and west and associated with boudinaged layers dominate at this exposure.

4.3. Unit 1-B middle

Unit 1-B middle is up to 25 m thick and rests on unit 1-B lower by means of an erosive surface (Fig. 6F). It is composed of two facies associations bounded by a distinct sharp contact (Fig. 3A). The basal association is up to 20 m thick and comprises a sandy-gravelly, coarsening-upward interval. Beds are tabular and consist of well- to poorly-sorted, cross-stratified sandstones and conglomerates as well as sandy, clast-rich, massive diamictites (F3, F7, F8; Fig. 7A, B). This facies association is not regularly distributed through the study area

and, at some localities, is absent or has a reduced thickness. Laterally discontinuous, soft-sediment grooved and striated surfaces with small sand slumps inside some grooves are present on some sandstone bedding planes (Fig. 7C).

The upper association is a fine-grained succession (Fig. 7D-F) mainly composed of intercalated beds of current- and climbing-rippled sand-stones (F9, F10), laminated heterolithics (F12), massive, sandy mudstones with dispersed outsized clasts (F13), and massive to faintly-stratified, clast-rich diamictites (F5). Beds of muddy, fine-grained heterogeneous sandstones with relicts of current ripples (F14) occur in between strata. Outsized clasts up to cobble size occur throughout the fine-grained beds. Paleocurrents from both facies associations that form unit 1-B middle display an asymmetric bimodal pattern with a main mean vector to the southwest (241°) and a subordinate one to the northeast (Fig. 3C).

This unit exhibits an upward increase in deformation intensity from a non-deformed basal portion of the sandy-gravelly association to a highly sheared and folded fine-grained association at the top (Fig. 3A). At locality 4 (Eng. Bley station), the upper portion of the sandy-gravelly association and the base of the fine-grained association display gentle to open, symmetric to somewhat asymmetric, synclines and anticlines that are truncated by mega-scale subhorizontal shear surfaces (Fig. 8A, B). Such folds are parasitic of a mega-scale (~400 m-long) gentle anticline and their asymmetry shows a vergence to the west (273° mean azimuth; Fig. 3C). Some low-angle imbricated thrusts occur in the uppermost sandy-gravelly strata.

The entire fine-grained association presents subhorizontal cm-scale shear surfaces (Fig. 8C). Towards the top, strata of the fine-grained association are gently- to open-folded, boudinaged, and thickened/thinned mainly where interbedding between fine-grained sandstones and

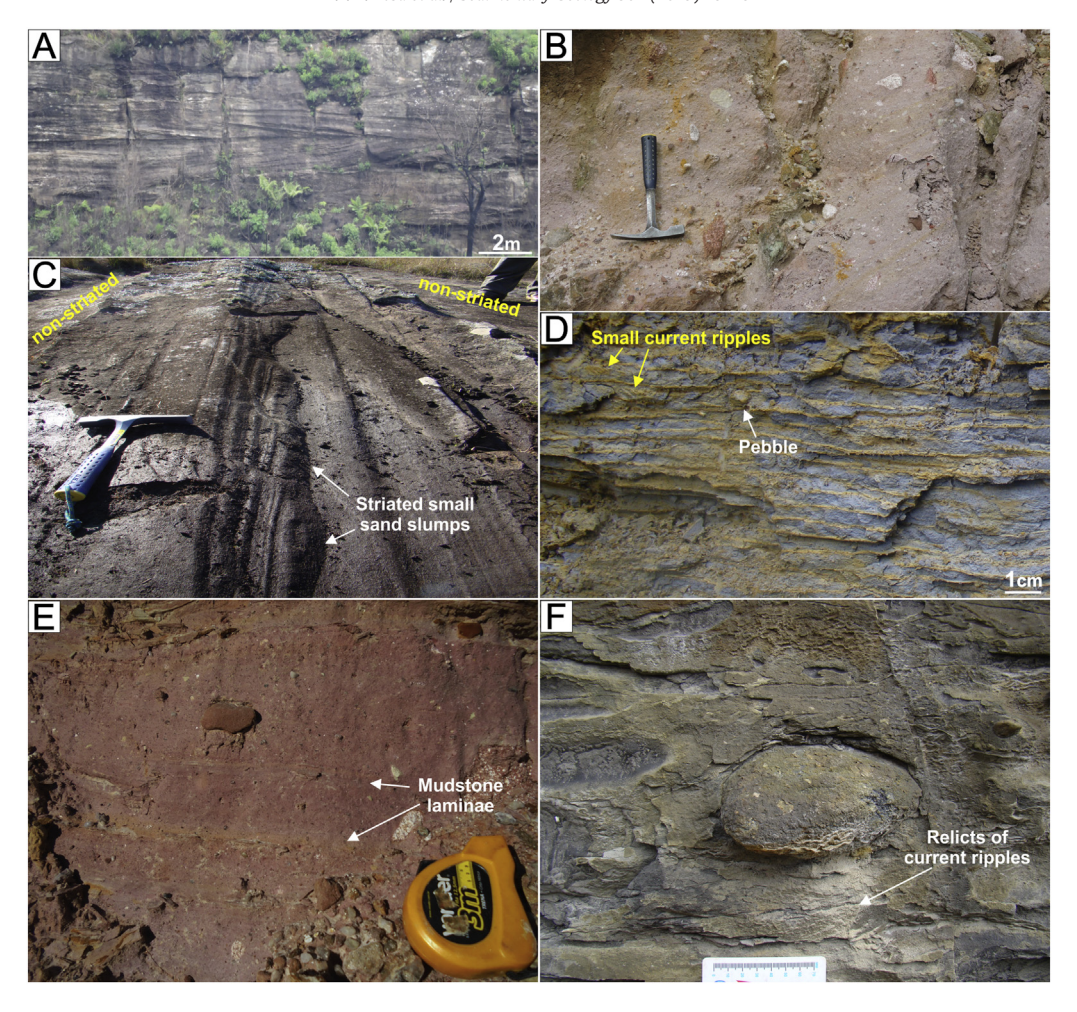


Fig. 7. Main sedimentary facies of unit 1-B middle. (A) Large-scale cross-stratified sandstones and conglomerates (F7, F8); (B) massive, sandy, clast-rich diamictites (F3) that dominate at the top of sandy-gravelly association; (C) soft-sediment striated surface developed on top of sandstone beds with a cross-cutting pattern with small striated slumped sand directed into a major trough; (D) heterolithic deposits with cm-thick sandstone/mudstone pair containing small current ripples (F12). White arrows indicate pebbles; (E) faintly-stratified, clast-rich diamictite with stratification defined by mudstone laminae (F5); (F) outsized Furnas Formation sandstone clast immersed in muddy, fine-grained sandstone with relicts of current ripples (F14).

sandy mudstones takes place. Beds of current-rippled, fine-grained sandstones are better preserved and beds of sandstones with a higher mud content contain relicts of current ripples cut by cm-scale subhorizontal shear planes and mm- to cm-scale reverse faults. The cm-scale shear surfaces measured from the fine-grained association have a mean vector dipping at low angles towards the east/northeast (N81/10; Fig. 3C). This indicates a westward/southwestward applied stress field similar to the folded fine-grained and sandy strata from unit 1-B lower.

4.4. Unit 1-B upper

The upper interval of unit 1-B is an up to 40 m-thick, erosive-based, sandy-gravelly succession that occurs throughout the ice-contact complex outcrop belt (Fig. 9A-C). The basal boundary is uneven, and at some places, the unit lies directly on the metamorphic basement. This unit is partially composed of amalgamated tabular beds of cross-stratified, well- to poorly-sorted sandstones and conglomerates (F7, F8), and current-rippled sandstones (F9). Paleocurrents from these beds are consistent with orientations to the northwest (322° mean azimuth; Fig. 3C). The sandstones and conglomerates are associated with massive, sandy, clast-rich diamictites (F3), massive sandstones (F11), and massive conglomerates with metric mudstone rip-up clasts (F6). Rapid facies changes are observed in outcrop scale both vertically and laterally. Massive m-scale tabular beds of sandy diamictites grade upward to dm-scale beds of massive, medium-grained sandstones and

current-rippled sandstones (Fig. 9C). Tabular beds of cross-stratified conglomerates grade laterally to gravelly sandstones in a downflow direction. Laterally discontinuous, soft-sediment striated surfaces containing marginal berms (i.e., lateral rims generated by sediment displacement during scour) are common on sandstone and conglomerate bedding planes (Fig. 9D). In general, they reach tens of m² in area but can be up to 450 m².

The unit 1-B upper exhibits a heterogeneous deformational pattern both vertically and horizontally. In general, the base of the interval is either not deformed or slightly deformed, and deformation structures become more frequent towards the top. However, at localities 11 and 13 the basal strata are highly deformed and display tight to close folds cut by medium- to low-angle cm-scale shear planes (Fig. 3B).

At locality 13 (Bassani sand pit), sandy-gravelly strata are affected by large (\sim 20 m-long), open symmetrical to asymmetrical synclines and anticlines that are intercepted by mega-scale thrust surfaces (Fig. 10). The thrusts are overall subhorizontal but because of undulations, dips of up to 60° can be found locally. Internally, these thrusts define shear zones up to 40 cm thick and displaying cm- to dm-long sigmoid sand bodies surrounded by a fine-grained matrix.

At localities 6 to 10, which consist of a series of 200 m long railroad cuts, the sandy-gravelly association shows a clear upward increase in deformation and a decrease in the preservation of original stratification. Slightly asymmetrical open folds associated with thrust surfaces occur in sets of beds in the middle portion of the unit and display northwestward kinematics (Fig. 11A, B). In the topmost portions, sets of beds

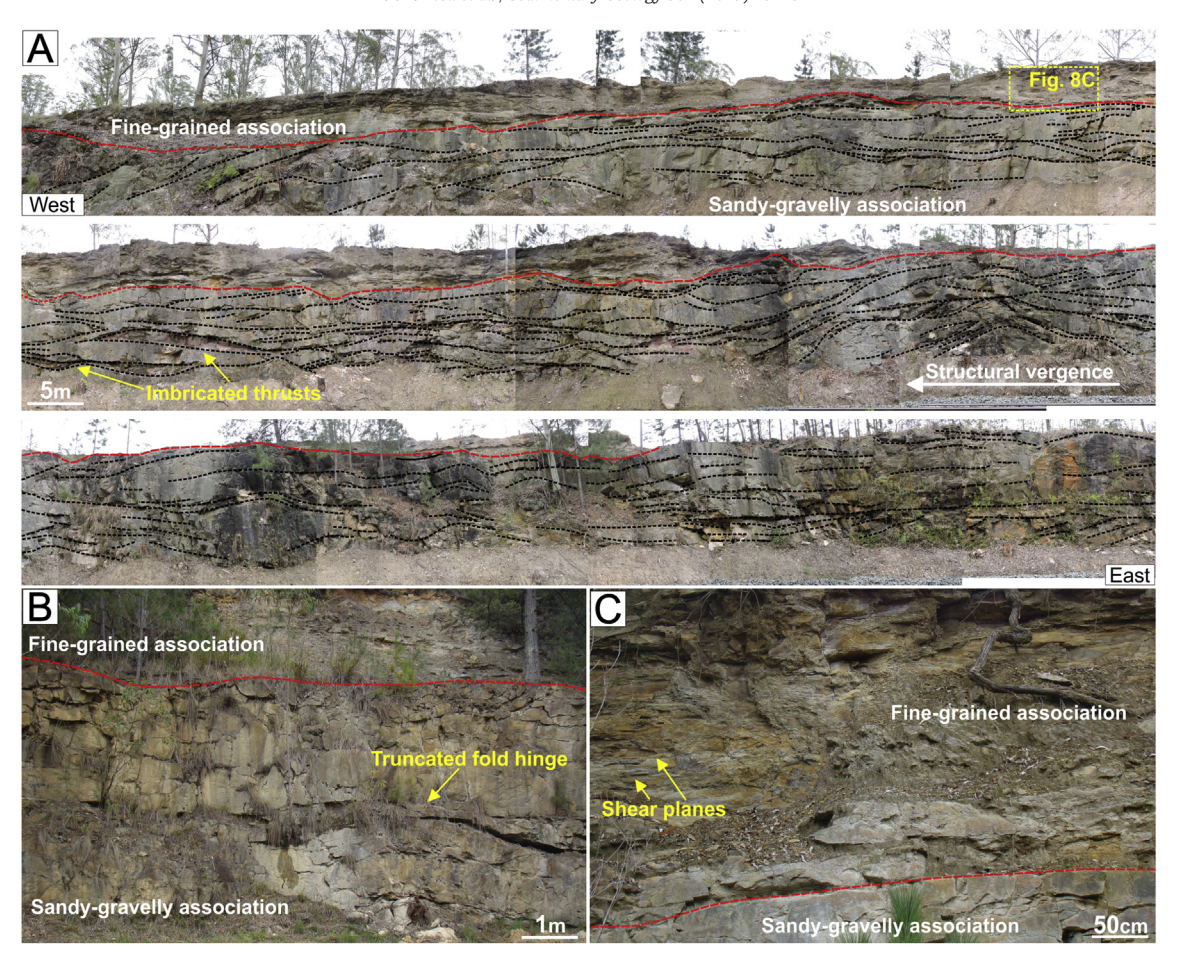


Fig. 8. Deformational patterns of unit 1-B middle in a railroad cut at Eng. Bley station (locality 4). (A) 300 m-long west-east photomosaic of the western limb of a mega-scale gentle anticline. The dashed red line represents a mega-scale shear surface that separates the gently- to open-folded, sandy-gravelly strata (black lines) below from the sheared, fine-grained association above; (B) detail of a truncation surface in between the sandy-gravelly association cutting the hinge of an open anticline; (C) detail of the basal portion of the fine-grained association composed by highly-sheared, muddy, fine-grained sandstones (F14). (For interpretation of the references to color in this figure legend, the reader is referred to the web version of this article.)

become more deformed with current-rippled sandstone beds disposed in isoclinal folds (Fig. 11C). Common structures at this level are small normal faults dipping to the northwest that are associated with boudinaged layers of fine-grained sandstones (Fig. 11D). Randomly-oriented fractures, mainly in a subvertical position, also occur in some places.

A muddy to intermediate, clast-poor, massive diamictite facies with mm-spaced subhorizontal shear surfaces and clasts oriented parallel to the shear trend (F2; Fig. 11E) is present in the top of unit 1-B upper. At locality 13, the diamictite occurs in lenticular slabs up to 6 m thick placed within the upper strata of the sandy-gravelly association (Fig. 10, 11F). This diamictite contains abrupt subhorizontal sheared contacts with slickensides (Fig. 11G). At locality 10, the same diamictite facies appears as a sheet-like body with a diffuse lower contact grading from underlying deformed sandy-gravelly facies (Fig. 3A).

Both sandy-gravelly facies and muddy diamictites of this unit exhibit deformational structures with a primary vergence towards the northwest. The mm-spaced shearing inside muddy diamictites has a consistent dip direction to the southeast (132/10). This same vergence direction is also indicated by fold asymmetry in the sandy-gravelly succession (300° mean azimuth) and by the dip towards the southeast of slickensides (321° mean azimuth transport; Fig. 3C).

5. Depositional settings

The examined succession alternates between slightly deformed/non-deformed and highly deformed strata. In the highly deformed intervals,

shearing destroyed much of the original depositional structures, leaving only relicts that can be used to interpret original sedimentary processes and depositional environments. Nevertheless, sedimentary facies and stacking patterns were used to group these deposits into three facies associations related to glacial environments: (i) subglacial tillites (subglacial); (ii) proximal grounding-line fan (ice-marginal); and (iii) distal grounding-line fan (proglacial) (Fig. 12). These associations are stratigraphically recurrent (Fig. 3A), indicating environmental cyclicity.

5.1. Subglacial tillites

Sandy diamictites of unit 1-A (F1) were previously interpreted as a subglacial deforming layer (i.e., subglacial tillites) related to a single event of glacial advance over the Devonian bedrock (Vesely et al., 2015). The sandy matrix of the diamictite is interpreted as a result of abrasion and assimilation of the Devonian Furnas sandstones that compose the paleobedrock.

Since the glacial advances continuously transmit stress to their basal deforming layers, distinguishing processes operating within the subglacial zone (i.e., melt-out, lodgement, sliding, subglacial meltwater flows) was not possible. Therefore, the massive/homogeneous character of the diamictites and the subhorizontal anastomosing shear planes merely suggest a glacier coupled to its bed that moved mostly by subglacial sediment deformation and gave rise to subglacial traction tillites (van der Meer et al., 2003; Evans et al., 2006).

The upper surfaces of the diamictites containing flutes, grooves and ridges were generated at the ice/sediment interface due to plowing

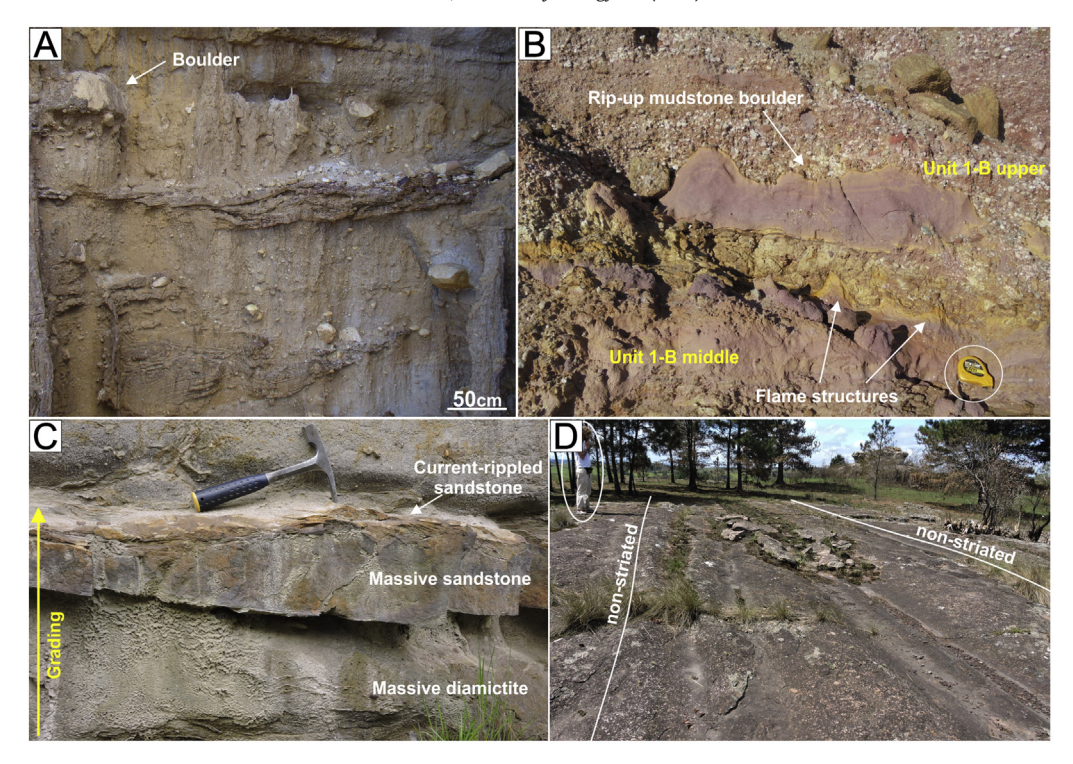


Fig. 9. Sedimentary facies of unit 1-B upper. (A) Deformed strata of massive, sandy, clast-rich diamictites with faceted clasts up to boulder size (F3); (B) flame structures at the contact between unit 1-B middle below and 1-B upper above containing conglomerates with a m-scale rip-up mudstone boulder (F6); (C) beds with normal grading from massive, sandy diamictites to current-rippled sandstones; (D) laterally restricted soft-sediment grooved surface over non-deformed sandstones with shallow grooves inside an 85 m-long, 5 m-wide trough.

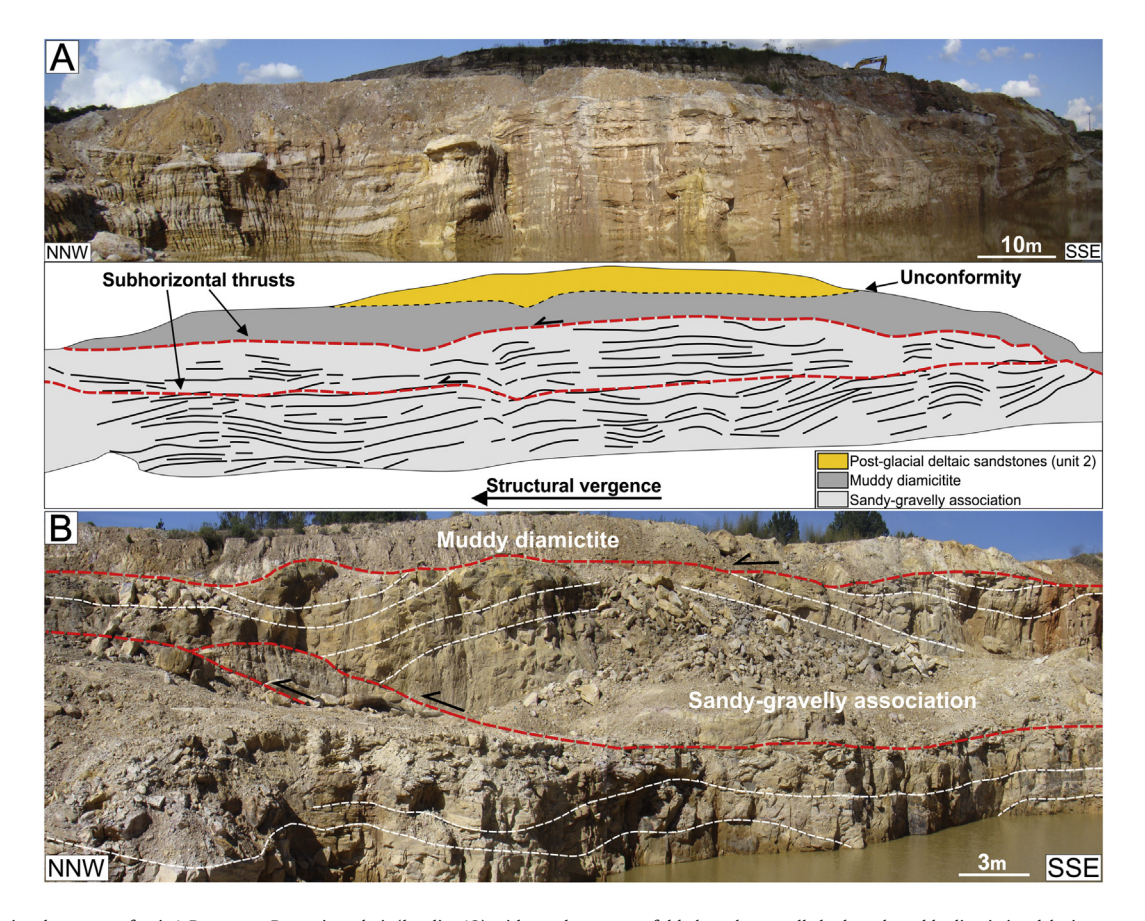


Fig. 10. Deformational patterns of unit 1-B upper at Bassani sand pit (locality 13) with gently- to open-folded sandy-gravelly beds and muddy diamictite slabs juxtaposed by mega-scale subhorizontal shear surfaces (red dashed lines). (For interpretation of the references to color in this figure legend, the reader is referred to the web version of this article.)

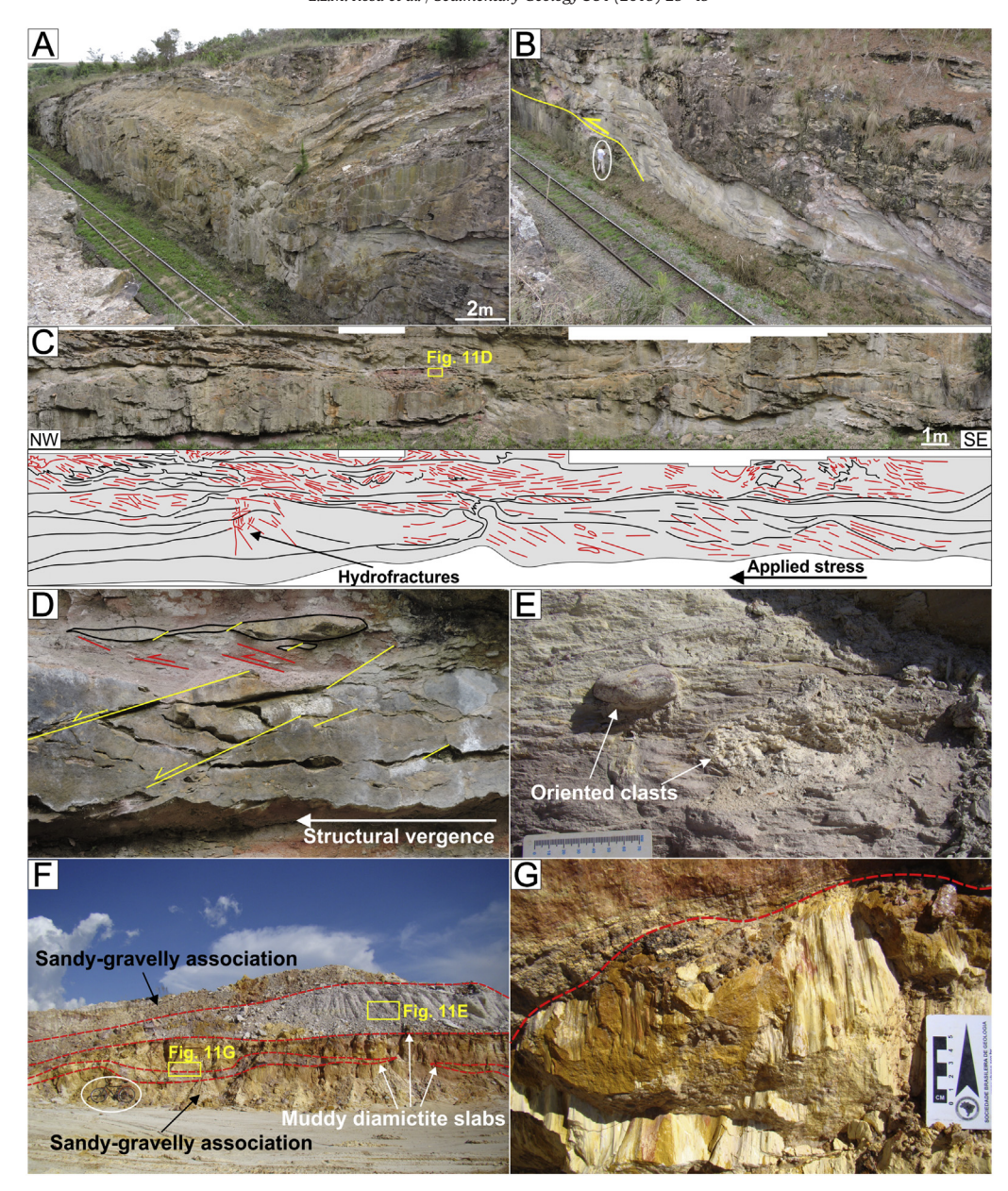


Fig. 11. Deformational patterns of unit 1-B upper. (A) Sandy-gravelly facies arranged in a large, open, asymmetrical syncline with a truncated limb associated with (B) thrust surface shown by a yellow line; (C) sandy-gravelly association cropping out in a railroad cut at locality 9. Bedding remnants (black lines) of sandy-gravelly strata that are folded, boudinaged and cut by low- to moderate-angle, cm-scale shear surfaces (red lines); (D) small-scale normal faults (yellow lines) associated with fine-grained sandstone boudins and cm-long shear planes (red lines); (E) muddy, clast-poor diamictite with subhorizontal mm-thick shear surfaces and faceted clasts oriented parallel to shearing (F2); (F) macro-scale muddy diamictite slabs between the top portions of sandy-gravelly association; (G) slickensided contact (red line) between muddy diamictite and sandy-gravelly facies. (For interpretation of the references to color in this figure legend, the reader is referred to the web version of this article.)

when sediment strength was exceeded, and the ice began to slide over the bed (Benn and Evans, 2010). The subglacially-abraded/plucked bedrock and the up to 7 m-thick deforming layer are evidence for a predominantly wet-based basal thermal regime and relatively fast glacier flow by a combination of soft-bed deformation and bedrock abrasion (Bennett and Glasser, 2009).

All the observed subglacial striated surfaces are flat and laterally extensive, unlike other irregular subglacial erosional surfaces (i.e., gouges, troughs, and streamlined bedforms) documented in other portions of the Paraná Basin (e.g., Almeida, 1948; Fallgatter and Paim, 2017). These characteristics suggest a relatively flat glacier/bedrock interface and that glaciers were unconstrained by topography. In addition, the spatial distribution of subglacial striated surfaces both on Devonian sandstones and over the subglacial tillites, as well as the shear plane orientations, ranging from the north/northwest to north/northeast

(Fig. 2) evidences a radial flow pattern. Therefore, it can be related to an advancing glacier with a lobate terminus similar to Pleistocene ice lobe margins (e.g., Colgan and Mickelson, 1997). The emplacement of thick till sheets depends firstly on the location within the subglacial zone and typically occurs within subglacial environments that are relatively close to the ice margin (Boulton and Deynoux, 1981; Boulton, 1996). Taking this into account, the evidence for ice/sediment coupling and the radial pattern of subglacial striated surfaces suggests that the subglacial traction tillites of unit 1-A were emplaced in the subglacial outer zone, thus representing the marginal portions of an ice lobe.

The muddy to intermediate, clast-poor diamictites (F2) at the top of unit 1-B lower and 1-B upper are interpreted as having been emplaced within the subglacial zone because of the presence of significant shearing and their stratigraphic position on top of deformed strata. Unlike unit 1-A, these diamictites were formed subglacially when an advancing

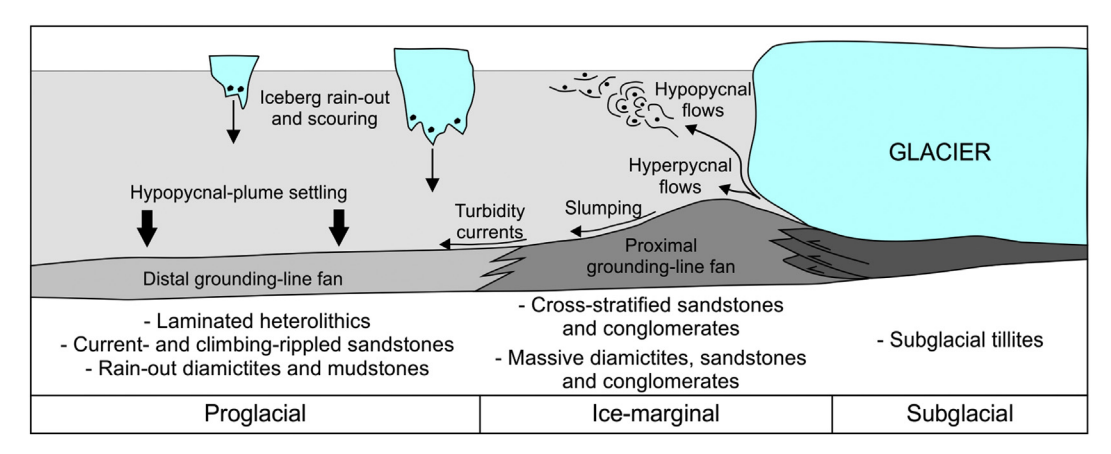


Fig. 12. Model of main depositional processes operating at different zones of a grounded temperate glacier system and their main respective sedimentary products (after Eyles et al., 1985; Ingólfsson, 1987; Hart and Roberts, 1994). Individualized facies associations are inserted in the subglacial (subglacial tillites), ice-marginal (proximal grounding-line fan) and proglacial (distal grounding-line fan) zones.

glacier overrode and homogenised pre-existing unconsolidated deposits (e.g., Hart, 1995).

5.2. Proximal grounding-line fan deposits (ice-marginal association)

The amalgamated, coarsening-upward, sandy-gravelly intervals that compose the bulk of the middle and upper portions of unit 1-B, as well as a localized sandy interval on top of unit 1-B lower, contains facies compatible with high-energy sedimentation processes, such as density flows (hyperconcentrated-to-concentrated character; Mulder and Alexander, 2001) and energic bedload-dominated currents (Table 1). Sets of current-rippled sandstones strata generated by weak currents under lower flow regime occur in between these higher energy beds, indicating temporal variation in flow energy. Rapid lateral/longitudinal/vertical changes in facies and grain-size demonstrate flow deceleration, decreasing sediment concentration and expansion from a confined to an unconfined state in a subaqueous environment (e.g., Russell and Arnott, 2003).

Unlike the laterally extensive subglacial soft-sediment surfaces over the unit 1-A diamictites, the soft-sediment surfaces over sandstones and conglomerates are interpreted as iceberg-keel scour marks due to: (i) their laterally restricted distribution of grooves and ridges; (ii) the presence of marginal berms; (iii) the presence of small-scale slumped and striated sandstone lobes in between the main grooves; and (iv) the fact that they occasionally occur on non- to slightly-deformed sandstone and conglomerate beds (e.g., Woodworth-Lynas and Dowdeswell, 1994; Eyles et al., 2005; Vesely and Assine, 2014).

Sedimentation characteristics are consistent with coarse-grained, grounding-line fan systems fed by sediment-laden meltwater flows at the grounding zone of a temperate, tidewater, calving glacier margin (e.g., McCabe and Eyles, 1988; Powell and Alley, 1997). The sandy, clast-rich, diamictite facies (F3) are attributed to the most proximal area in relation to the tunnel stream mouth (i.e., zone of flow establishment; Powell, 1990). Gravity-driven resedimentation in the form of low-magnitude slumps at the grounding-line fan slope is also interpreted to have been a formative mechanism for massive sandstones (F11) and normal-faulted diamictites (F4) interbedded with the meltwater-fed facies (Powell and Domack, 2002).

5.3. Distal grounding-line fan deposits (proglacial association)

The depositional characteristics of the proglacial association are poorly preserved in most places due to soft-sediment deformation. The fine-grained strata that predominate in unit 1-B lower and occur at the top of unit 1-B middle were generated by a range of processes. These processes point to deposition at the proglacial zone of a grounded,

temperate, tidewater glacier and place these deposits in the distal setting of the grounding-line systems (Eyles et al., 1985; Molnia, 1989; Powell and Domack, 2002).

The main characteristic of this association is the dominance of dmthick interbeds of outsized clasts-bearing, fine-grained facies, which are attributed to have been generated mainly by low-energy sedimentation processes (Table 1). These processes include: (i) low-energy tractive currents; (ii) settling of suspended fine sediment from hypopycnal plumes emanated from the ice margin; (iii) rain-out of ice-rafted debris (IRD); and (iv) resedimentation in the form of turbidity flows.

The outsized clast-bearing, massive mudstones/sandy mudstones (F13) and the clast-rich, massive to faintly-stratified diamictites (F5) are interpreted as the product of rapid settling of fine outwash sediments (i.e., hypopycnal plumes) plus IRD rain-out. This is due to the faint stratification of diamictites defined by mm-thick mudstone laminae, which suggests that the laminae were deposited during fluctuations in the balance between mud settling and IRD rain-out (Eyles et al., 1985; Powell and Molnia, 1989; Powell, 1994).

Mm- to cm-thick heterolithic facies (F12) suggest deposition by turbidity flows associated with settling of hypopycnal plumes and minor IRD rain-out. This interpretation is based on: (i) minor truncations between laminae sets and mudstone rip-up clasts indicating erosion between each turbidity flow; (ii) mudstone laminae that are sometimes thicker than sandstone laminae and contain embedded clasts of very coarse sand to pebbles, occasionally deforming the laminae; (iii) the close association with fine-grained, climbing-rippled sandstones; and (iv) the occurrence of small current ripples in the sand laminae (e.g., Walker, 1965; Stow and Shanmugam, 1980; Molnia, 1989). Taking these features into account, we argue against lacustrine seasonallyinduced varve formation by sediment decantation (Brauer, 2004; Fitzsimons and Howarth, 2018). The lack of varve deposits and the abundance of deposits generated by settling of buoyant hypopycnal plumes, which are facilitated due to the density difference between meltwater and seawater, suggest deposition in a glaciomarine setting.

6. Glaciotectonics

Although with variable intensities and structural styles, penecontemporaneous, soft-sediment deformation is present throughout the studied succession. Distinguishing between mass-transport deposit deformation and glaciotectonics in the geological record is difficult because their structural assemblages can be identical (Visser et al., 1984; Eyles et al., 1985; van der Wateren et al., 2000; McCarroll and Rijsdijk, 2003). Mass-transport deposits are internally characterized by distinct extensional (upslope) and compressional (downslope) domains (Alsop et al., 2017; Sobiesiak et al., 2017). Shear zones are restricted to the base of mass flows and to some internal sliding planes. On other hand, the ice-marginal deformed zone is dominated by compressional deformation whereas simple shear prevails in the subglacial zone (Bennett, 2001; McCarroll and Rijsdijk, 2003; Phillips, 2018).

Similar deformation patterns can be produced in unconsolidated to semi-consolidated sediments either due to overriding by a glacier or by a mega-scale mass flow. In these basal shear zones, deformation profiles usually show an upward increase in strain towards the base of the glacier/mass flow (Hart and Boulton, 1991; van der Wateren, 2002; Sobiesiak et al., 2018).

In our study, the evidence for a glaciotectonic origin includes a close association with glaciogenic features such as striated surfaces, striated and bullet-shaped clasts, ice-rafted outsized clasts, and iceberg keel scour marks. In addition, the overall consistency of measured structures (Fig. 3C) suggests highly-confined stress fields for deformation, which differs from slumps where soft-sediment deformational structures are often randomly distributed due to unconfinement and the influence of bottom topography (Hart and Roberts, 1994; McCarroll and Rijsdijk, 2003; Dykstra et al., 2011). Also, the dominance of simple shear and compressional shear deformation together with the lack of extensional deformation domains support the glaciotectonic interpretation for these deposits (Visser et al., 1984; Hart and Roberts, 1994; Martinsen, 1994).

Except for the small normal faults located within tabular diamictite beds (F4) interpreted as the result of small-scale slump processes, the structures described herein are interpreted to have been generated by stress directly transmitted from advancing glaciers onto unconsolidated to semi-consolidated sediments (Aber et al., 1989; Phillips, 2018). The assembly of glaciotectonic structures shows intervals deformed in simple-shear-dominated subglacial settings as well as under a compressional regime at the glacier margin (McCarroll and Rijsdijk, 2003).

In addition to the diamictites of unit 1-A, part of the unit 1-B lower strata as well as the muddy diamictite on top of unit 1-B upper are likely to have been generated subglacially and acted as the basal deforming layer (Evans et al., 2006; Menzies et al., 2018). A typical idealized vertical sequence/continuum of subglacially simple-shear-deformed sediments during glacial overriding would show an increase in strain towards the glacier sole and a transition from glaciotectonites to a homogeneous tillite (Hart et al., 1990; Hart and Boulton, 1991; Evans et al., 2006). This matches the observed sequence of unit 1-B lower at locality 2. At this location, there is an upward transition from a bottom zone dominated by rootless isoclinal folds, passing to a zone dominated by subhorizontal shear planes with boudinaged and disrupted sandy layers, towards homogenised diamictites on top.

In addition to the subglacially-imposed deformation on unit 1-B lower, the proximal grounding-line strata exposed at localities 16 and 17 show an assemblage of gentle to close folds, boudinaged strata, and reverse and normal faults that are attributed to compressional shear (McCarroll and Rijsdijk, 2003). This suggests that part of unit 1-B lower was not overridden by the glacier. Rather, these features are indicative of the sediments were deformed in an ice-marginal setting, corresponding to the generation of a push moraine.

Unit 1-B middle was deformed at the ice margin during an episode of ice advance and represents the distal portion of the deformed foreland. This push moraine was described at localities 3 to 5 where ice-marginal sandy-gravelly and proglacial fine-grained deposits contain low amplitude folding and thrusting. The gentle and open folds observed at these outcrops are parasitic folds of mega-scale synclines and anticlines. Subhorizontal truncation surfaces in between the sandy-gravelly deposits, that cut sets of folded strata, are likely interpreted as mega-scale shear surfaces related to nappe-style compressional deformation (Kluiving, 1994; van der Wateren, 1995). In this model, nappes are slightly deformed internally and bounded by subhorizontal, simple-shear-dominated zones. Imbricated, low-angle thrusting occurs at the base of some nappes especially in their distal extremities (Bennett, 2001). Simple-shear-dominated horizons and intrastratal displacement facilitated by contrasts in stratal composition (van der Wateren, 1985;

Murray, 1994) can be observed at the contact between proglacial finegrained facies and the underlying grounding-line sandy-gravelly strata, as well as in between fine-grained interbeds containing subhorizontal mm- to cm-scale shear surfaces and heterogeneous matrix material (i.e., F14).

The push moraine that is in the deformed grounding-line fan deposits of unit 1-B upper is likely related to a thrust-fold style (Croot, 1987) and has a complex assembly of glaciotectonic structures. High strain is confined to thrusts that bound some non- to moderately-deformed sets of sandy-gravelly strata. These thrusts are sometimes rooted at the base of the sandy-gravelly association and are possibly related to a décollement surface that underlies the whole push moraine complex (Boulton et al., 1999). Folds related to thrusting are common and range from close to tight with an asymmetric profile with a northwestward vergence direction.

Homogeneous, sheared, muddy diamictites located in mega-slabs in between the top strata of unit 1-B upper at locality 13 show slickensided sheared contacts with surrounding sandy-gravelly strata. These diamictites are attributed to a basal deforming layer and their emplacement as slabs was likely due to transmitted stress, which is common in push moraines at the subglacial to ice-marginal transitional zone (Boulton, 1996; van der Wateren, 2002). At outcrops corresponding to the top strata of this unit at the railroad track (localities 9 to 10), there is superimposition of simple-shear-dominated structures over compressional-deformed strata that progressively grade upwards to a homogeneous massive diamictite with a diffuse basal contact. Brittle fractures are analogous to some fractures described from Cenozoic deposits (Rijsdijk et al., 1999, 2010) that are related to upward water escape (i.e., hydrofracturing) caused by subglacial shearing of watersaturated sediments. At the Witmarsum locality, few outcrops of unit 1-B upper are available, and the sandy-gravelly strata are deformed and capped by a muddy sheared diamictite. We conclude that the glacier overrode the deposits at this locality and advanced northwestward across the study area.

7. Palynology and palynostratigraphy

Palynology was examined in two samples from the laminated heterolithics located at the base of unit 1-B lower (locality 2, sample BN-1) and from muddy, fine-grained sandstone in the upper portion of unit 1-B middle (locality 4, sample BN-2) (Fig. 3A). Devonian-restricted prasinophyte, acritarch, chitinozoan and miospore species were identified and are considered as reworked material from the underlying Devonian units (Ponta Grossa and Furnas formations).

The identified palynomorph assemblage is almost entirely composed of miospores but also includes an alga and an acritarch species (Fig. 13). This assemblage differs from previously described Pennsylvanian and earliest Permian assemblages and corresponding biozones from all portions of Itararé Group, because: (i) species of pollen grains are absent, and (ii) no guide species of Daemon and Quadros (1970) and Souza (2006) zonation were recognized. On other hand, the autochthonous assemblage is well documented in Mississippian strata throughout Gondwanan basins (e.g., Césari and Gutiérrez, 2000; di Pasquo, 2007a, 2007b; Pérez Loinaze, 2008a, 2008b; Playford and Melo, 2012; Playford and Mory, 2017) and Euramerican sequences (e.g., Higgs, 1990; Owens et al., 2004).

As shown in Fig. 13, the autochthonous assemblage comprises miospores with their last appearance datum and first appearance datum in the late Visean and early Serpukhovian. This age range implies that the assemblage is likely associated with some well constrained Mississippian (middle Visean-early Serpukhovian) Gondwanan biozones such as: (i) Reticulastisporites magnidictyus-Verrucosisporites quasigobbettii (MQ Biozone; Pérez Loinaze, 2007; Césari et al., 2011); (ii) Reticulatisporites magnidictyus (Mag Biozone; Melo and Loboziak, 2003; Melo and Playford, 2012); and (iii) Grandispora maculosa (GM Biozone; Playford, 2015; Playford and Mory, 2017), which have not

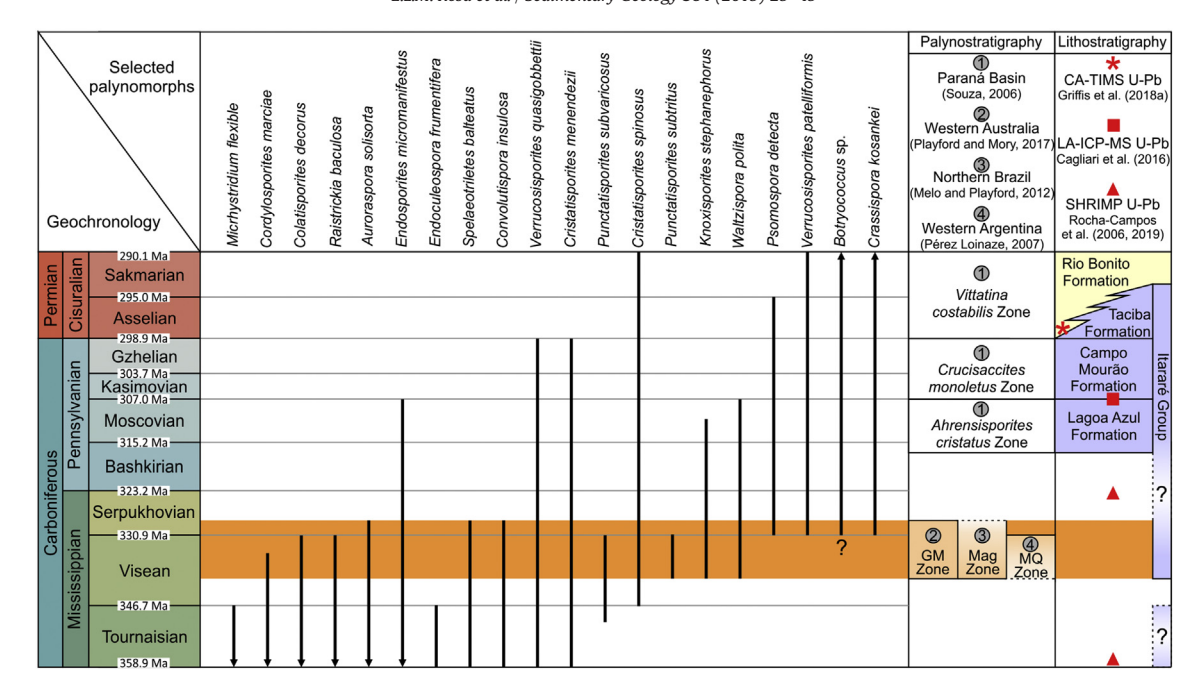


Fig. 13. Chronostratigraphic distribution of selected palynomorphs recorded from units 1-B lower and 1-B middle. Orange-shaded zone indicates the middle Visean-early Serpukhovian interval in which strata of the unit 1-B lower and middle were deposited and correlated to other Gondwanan biozones.

been yet recognized in the Itararé Group. The absence of monosaccate pollen grains in the identified assemblage denotes a pre-late Serpukhovian age since pollen grains were introduced globally during the Serpukhovian and became abundant in the late Serpukhovian (Clayton et al., 1990; Playford, 2015). By this means, it is argued that the depositional age of the unit 1-B lower to the unit 3 of Vesely et al. (2015) can be constrained between the middle Visean-Moscovian/Kasimovian boundary.

The acritarch *Micrhystridium flexible* ranges in age from the latest Devonian (Famennian) through the Tournaisian (Richardson, 2008). In addition, the miospore *Endoculeospora frumentifera* was only identified and constrained in Tournaisian strata in the Amazonas Basin of northern Brazil (Melo and Playford, 2012). Both palynomorphs might have been reworked from possible older strata that were eroded and correspond to the glacial episode that deposited the tillites of unit 1-A. It is important to note that SHRIMP U—Pb Famennian-Tournaisian ages (356.9 \pm 22 Ma; 359.6 \pm 8.1 Ma) were mentioned by Rocha-Campos et al. (2006, 2019) from ash-fall deposits interbedded with shales of the lowermost Itararé Group in São Paulo State. However, the zircons were treated as detrital and the authors rejected the ages for being incompatible with the known ages of the Itararé Group (Fig. 13).

8. Glacial timing, cyclicity and paleoice flow

Considering the vertical changes in facies association and deformation patterns as well as erosive/glaciotectonic kineto-indicators, three major glacial cycles of advance and retreat in the lowermost portion of the Itararé Group can be defined for the study area (Fig. 3A). A graphic representation of these three cycles is shown in Fig. 14.

8.1. Glacial cycle 1 (GC1)

During glacial cycle 1 (GC1), a warm-based ice lobe advanced northward and abraded the underlying Furnas Formation and Precambrian basement. A sheet of sandy tillites (unit 1-A) was deposited subglacially on this unconformity at the outer subglacial zone. The modification of original strata by Phanerozoic reactivations of major basement fault systems (i.e., Lancinha Shear Zone; Fig. 2) (e.g., Castro et al., 2014) and by Mesozoic uplifting of the Ponta Grossa Arch (i.e., Strugale et al.,

2007) makes it difficult to deduce if there was a topographic control on glacial flow, as has been documented in other parts of the Paraná Basin (e.g., Fallgatter and Paim, 2017). However, the flat and laterally extensive surfaces associated with the basal unconformity points to a glacier unconstrained by topography, thus excluding fjord or topographically-controlled ice stream settings for this ice lobe.

Whether the glacier advanced on land or into a marine environment is still unclear. Trosdtorf et al. (2005) suggested the latter and inferred a rapid glacier retreat followed by meltwater-fed deltaic progradation (correlated herein to unit 1-B lower). Vesely et al. (2015), on the other hand, interpreted these deltaic sediments as having filled a small moraine-dammed lake that developed in front of a retreating terrestrial glacier. However, paleocurrents collected here from proglacial deposits that immediately overlie the tillites (i.e., unit 1-B lower) indicate sediment transport towards the southwest and a glacial source located to the northeast. This indicates that the water body was not filled by sediment derived from the same retreating ice margin that produced the basal tillite. This evidence for an apparent lack of deglacial deposits from this northward advancing ice lobe can be attributed to rapid glacier retreat (e.g., Boulton, 1990; Dowdeswell et al., 2015) or due to a temporal gap and subsequent erosion of the deglacial sequence.

The timing of this glacial advance and the time span between the subsequent glacial cycle is still unclear due to the lack of the GC1 deglacial sequence. However, the autochthonous palynomorph assemblage identified in the unit 1-B lower suggests an age not younger than middle Visean for GC1. The reworked palynomorphs restricted to the Tournaisian could be the result of erosion and reworking of the GC1 deglacial sequence, and a potential Tournaisian age for this glacial cycle cannot be excluded (Fig. 13).

8.2. Glacial cycle 2 (GC2)

The deposits associated with this glacial cycle occur stratigraphically above the tillites of unit 1-A and belong to the lower and middle portions of unit 1-B. Glacial cycle 2 (GC2) consists of a cycle comprised of two subordinate cycles (GC2-A and GC2-B) that represent minor ice margin fluctuations of a wet-based, tidewater ice lobe during the middle Visean-early Serpukhovian (stages II to VI; Fig. 14).

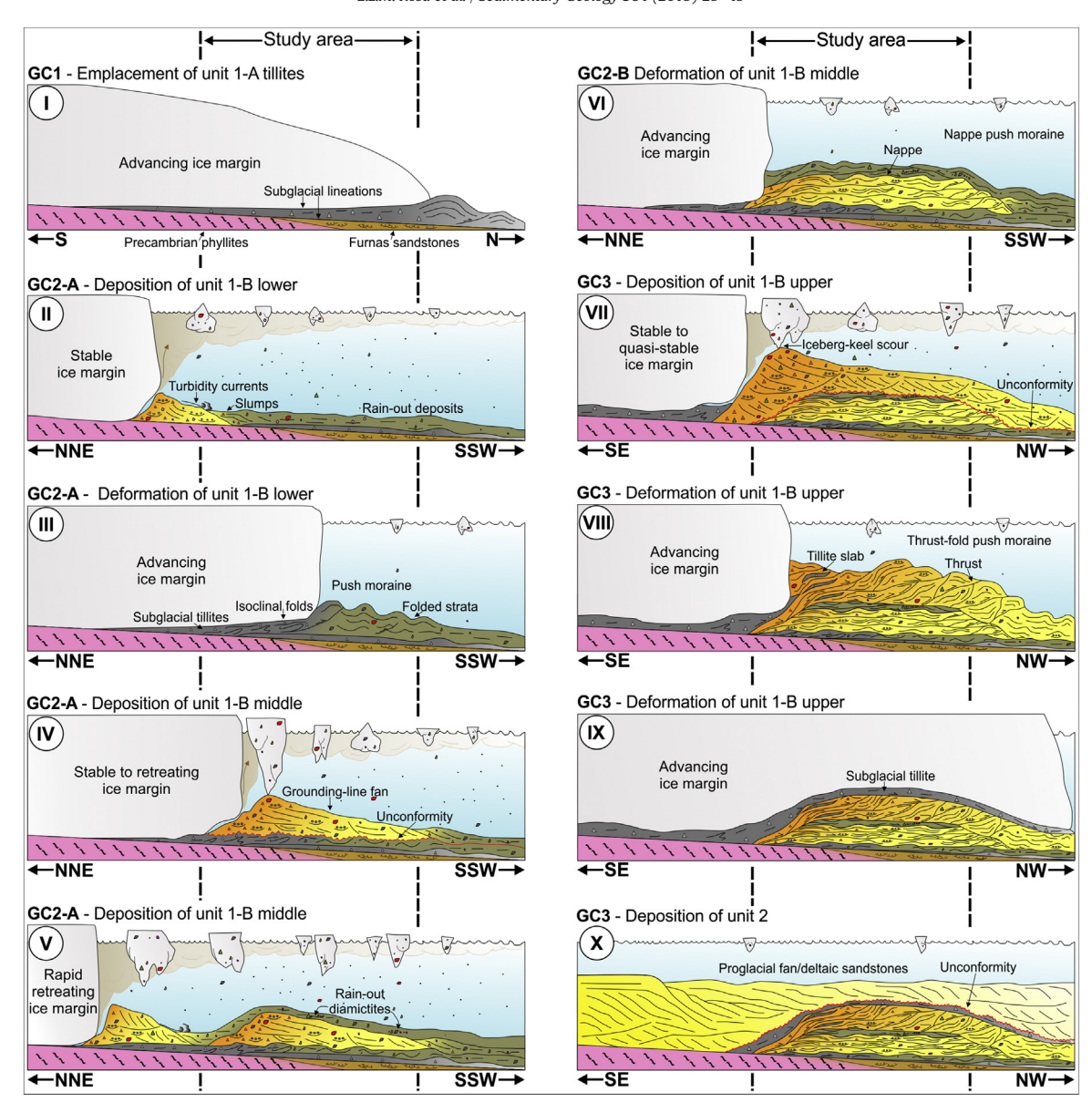


Fig. 14. Inferred evolutionary model of the ice-contact complex in the Balsa Nova region during the three glacial cycles discussed herein.

The establishment of fine-grained, proglacial deposition at the distal portions of grounding-line fans represents the beginning of GC2-A sedimentation within a subaqueous environment. Although no autochthonous, marine-related palynomorphs were recovered, the abundance of hypopycnal plume-settling deposits is suggestive of sedimentation within a marine environment.

Paleocurrents and the coarsening-upward pattern of unit 1-B lower imply the progradation of a proglacial system towards the southwest (243°) and an ice margin located to the northeast. Progradation is interpreted to have taken place during a long-term ice margin advance, which culminated with the glacier overriding most of the proglacial facies, as well as deforming some proximal grounding-line deposits at the ice margin. This deformation was responsible for forming push moraines. Evidence supporting this interpretation includes the fact that paleoice flow, deduced from subglacial glaciotectonic structures (i.e., shear planes and isoclinal folds), was parallel to sediment transport towards the west/southwest (260°).

A minor retreat phase marks the end of GC2-A and is recorded in the sandy-gravelly, proximal grounding-line fan deposits of unit 1-B middle which show a paleocurrent mean vector towards the southwest (241°). Internal facies variations are interpreted as the consequence of

fluctuations in meltwater discharge during a phase of stability or quasi-stability of the grounding zone during retreat. The sudden break between basal proximal grounding-line fan deposits and upper finegrained proglacial interval records a back-stepping of the groundingline fan due to a rapid change from a stabilized to retreating ice margin.

The subsequent deformation on the deglacial deposits of GC2-A is related to shear imposed by ice-push during a renewed ice advance. This advance event marks the onset of GC2-B, which gave rise to a push moraine characterized by folded strata truncated by mega-scale subhorizontal shear surfaces. These features are comparable to the nappe model of van der Wateren (1994, 1995). Stereographic analysis of folded strata and shear surfaces attributed to the GC2-B advance (261°–273°) indicates a westward/southwestward deformational vergence. Therefore, this episode can be related to a readvance of the same ice margin associated with GC2-A, implying in minor fluctuations of a westward/southwestward flowing ice lobe during GC2.

8.3. Glacial cycle 3 (GC3)

The ice retreat record of GC2-B is not preserved. This lack of preservation is believed to have been the combined result of low rates of

deposition and strong erosion during the onset of glacial cycle 3 (GC3). The initial phase of GC3 is recorded in the widespread proximal grounding-line fan deposits of unit 1-B upper, which overlie an unconformity that cuts underlying deposits of GC1 and GC2 and locally touches the Precambrian basement. This unconformity was probably generated by vigorous meltwater flows that scoured the unconsolidated to semiconsolidated substrate (e.g., boulder-sized rip-up clasts; Fig. 9B) and sourced high amounts of glacial debris to build a large grounding-line fan system at the margin of a temperate ice lobe (Ashley et al., 1991). A record of grounding-line fan sediments prograding to the northwest is indicated by the coarsening-upward pattern and a paleocurrent mean vector trending 322°. Phases of ice margin stability probably allowed the generation of a thick and laterally extensive, sandy-gravelly grounding-line fan (Dowdeswell et al., 2015).

The coarsening-upward pattern of facies and the vergence of glaciotectonic structures indicate that a glacier advanced to the northwest and progressively deformed the grounding-line deposits. This deformation involved compression due to ice-push at the ice margin and gave way to a thrust-fold dominated push moraine with tillite slabs in the proximal zone. Finally, these deposits were superimposed by simple shear subglacial deformation due to a progressive glacier overriding giving rise to the tillites placed on top of unit 1-B upper.

The simple-shear-dominated subglacial deformation indicates that glacier movement was controlled mainly by deformation of underlying deposits. These deposits, plus the subglacial tillites, are widespread and reach the northwesternmost portion of the study area. This suggests that, contrary to previous interpretations (e.g., Vesely et al., 2015), the ice margin advanced far beyond the area of the present study, probably reaching more internal zones of the basin during the GC3 maximum.

The retreat of this ice lobe and the deglaciation phase of GC3 are recorded by the glacially-influenced, non-deformed, proglacial fan to deltaic sandstones that overlie the ice-contact complex by an unconformity. These sandstones have paleocurrents to the northwest and contain ice-berg keel scour marks indicating that the ice margin was still in contact with the water body. The fact that the analyzed glaciogenic interval is directly overlain by proglacial fan to deltaic deposits and not by deepmarine deposits such as black shales and submarine slope mass-transport (e.g., Puigdomenech et al., 2014; Aquino et al., 2016) suggests that the ice-contact complex was generated in a relatively shallow marine environment, mainly controlled by fluctuations of grounded tidewater glaciers.

The timing of GC3 advance can be constrained to a period between the middle Serpukhovian-Moscovian/Kasimovian boundary as indicated by the palynomorphs from deep-marine rhythmites of unit 3 (Kipper et al., 2017) and by the assemblage recovered from GC2. The widespread unconformity that underlies GC3 is suggestive of a long-duration sedimentation gap after GC2. A late Serpukhovian-early Bashkirian age is suggested for GC3 ice lobe advance since it can be correlated to the LPIA glacial maximum observed through an δ^{18} O analysis of Visean-Guadalupian carbonates in China (Chen et al., 2016). This glacial peak is also well recognized and constrained in basins of western Argentina (Pérez Loinaze et al., 2010; Césari et al., 2011; Limarino et al., 2014). The decay of the GC3 ice lobe and the succeeding long-lived interglacial phase is recorded in the thick deglaciation sequence that transitions from deltaic deposits to deep-marine sedimentation towards the Moscovian/Kasimovian boundary (Fig. 1).

9. Implications for early LPIA paleogeography

During the Mississippian-Early Pennsylvanian, Gondwana moved around the South Pole and the eastern margin of the Paraná Basin was placed ~60° paleolatitudes (Lawver et al., 2011) (Fig. 15). LPIA successions and erosive landforms generated during this period were previously documented from basins in western Argentina, northern Brazil, and northern Africa (Caputo et al., 2008; Henry et al., 2008; Le Heron, 2017).

Paleoenvironmental reconstructions of ice masses during this period in the Paraná Basin and contiguous regions in Africa are absent due to the lack of age-corresponding strata.

Previous reconstructions indicate the presence of an ice center (i.e., Windhoek Ice Sheet; WIS) as the source of glaciers that carved glacial valleys (Martin, 1981) in northwestern Namibia and reached the eastern border of the Paraná Basin (e.g., Santos et al., 1996). The time of excavation of these valleys is still unconstrained, but it is likely related to the Late Pennsylvanian as the result of a waning stage of the WIS and base-level rise (Martin, 1961; Vesely et al., 2015). These valleys are better correlated with the Rio do Sul Ice Lobe and the subglacial landforms carved in the Santa Catarina State during the Late Pennsylvanian-earliest Permian (e.g., Fallgatter and Paim, 2017). Therefore, our interpreted glacial cycles are related to the maximum extent of the ice lobes derived from the WIS during the middle Visean-early Bashkirian and possibly during the Tournaisian (Fig. 15B).

The number of individual ice lobes in the eastern margin of Paraná Basin before the Late Pennsylvanian is still in debate. According to Crowell and Frakes (1975), França and Potter (1988) and Santos et al. (1996), the area of the present study was under the influence of a separate ice lobe (Paraná Ice Lobe) in relation to areas located to the north and south. Vesely et al. (2015) postulated that the deposition of the Pennsylvanian basal strata in Paraná State is better explained by two smaller ice lobes referred to as the Southern Paraná Ice Lobe (SPIL) and Northern Paraná Ice Lobe (NPIL). According to this model, the area of the present study was under the influence of the SPIL, which behaved as a fluctuating ice margin moving on emerged land towards the north and northwest (correlated herein to GC1 and GC3). In addition to the influence of the NPIL and SPIL on sedimentation in eastern Paraná Basin, the Kaokoveld Ice Lobe (KIL) is also invoked for the scouring and development of streamlined bedforms on Precambrian basement in São Paulo State (e.g., Santos et al., 1996).

Our results, however, suggest a more complex glacial scenario, involving the interaction and readvance of at least two distinct ice lobes in order to explain the stratigraphic complexity and changes of ice flow direction in time and space (Fig. 16).

Erosional features developed on the Itararé basal unconformity and basal tillites point to a strong northwestward ice flow trend (Rosa et al., 2016), however GC1 and GC2 ice flow directions in the Balsa Nova region deviate from this regional framework. This deviation could be a consequence of the radial flow pattern typical of advancing ice lobes (e.g., Colgan and Mickelson, 1997; Kehew et al., 2012).

Taking this into account, the GC1 could be related to a northward ice flow from the northern sector of the SPIL possibly during the Tournaisian (Fig. 16). The Tournaisian U—Pb ages obtained in the lowermost Itararé Group in São Paulo State (i.e., Rocha-Campos et al., 2006, 2019), even if from detrital zircons, are suggestive that the KIL was active earlier and could be responsible for generating the streamlined bedforms over Precambrian bedrock in São Paulo State (e.g., Almeida, 1948; Amaral, 1965; Rocha-Campos et al., 1968; Pérez-Aguilar et al., 2009) at the same time of the GC1 ice lobe advance.

After retreat of the SPIL, a marine incursion took place, followed by a major ice lobe advance (GC2) during the middle Visean-early Serpukhovian. A "Mississippian pre-Itararé" palynomorph assemblage recovered from the lowermost Itararé in a log nearby Engenheiro Maia (southwestern São Paulo State) was briefly mentioned by Caetano-Chang (1984). It suggests that the subglacial soft-sediment surfaces exhumed at this locality (Caetano-Chang et al., 1990) could be time-equivalent to the GC2 in Balsa Nova region and that both regions were affected by an advance phase of the NPIL (Fig. 16). In addition, as postulated by Vesely et al. (2015), the NPIL is also responsible for the deposition in Ventania region (northeastern Paraná State).

U—Pb detrital zircon ages from grounding-line fan deposits of unit 1-B upper (i.e., correlative to GC3) at the Bassani sand pit (Griffis et al., 2018b) demonstrate a major local-source contribution of Neoproterozoic grains likely derived from granitic rocks to the east.

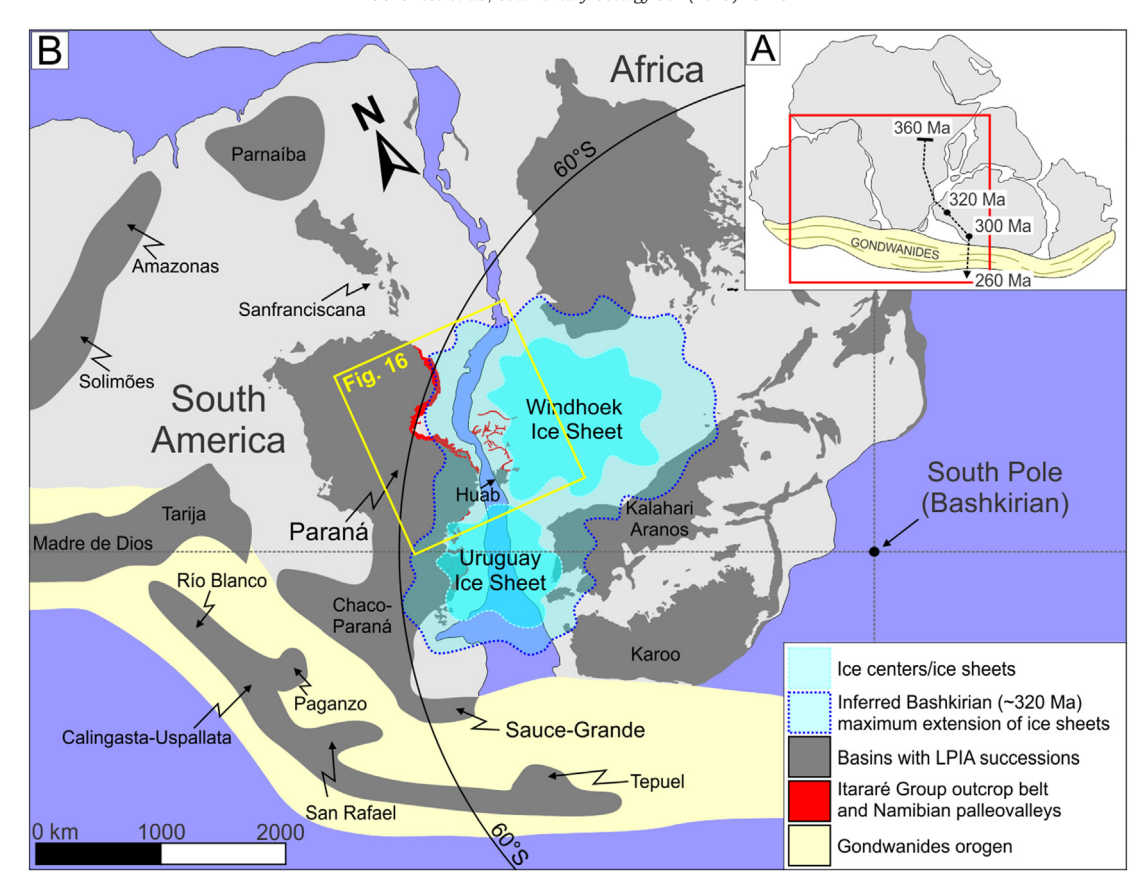


Fig. 15. (A) Gondwana map with the South Pole position during the LPIA (after Lawver et al., 2011) with (B) Gondwanic reconstruction of South America and Africa with main sedimentary basins that comprise the LPIA record. Inferred Mississippian-Early Pennsylvanian ice centers discussed in the text with their inferred maximum extent.

Such zircon grains could have been incorporated as glacial debris both by the NPIL and SPIL. Nonetheless, considering the regional ice flow pattern, the northwestward ice flow of GC3 is more likely explained by a renewed advance of the SPIL during the late Serpukhovian-early Bashkirian (Fig. 16).

Following the glacial cycles discussed herein, the final deposition of the Lagoa Azul Formation is characterized by a rise in sea level towards the Moscovian/Kasimovian boundary, as a consequence of major ice sheets waning during a long-lived interglacial period (Chen et al., 2016, and the sea level curves therein).

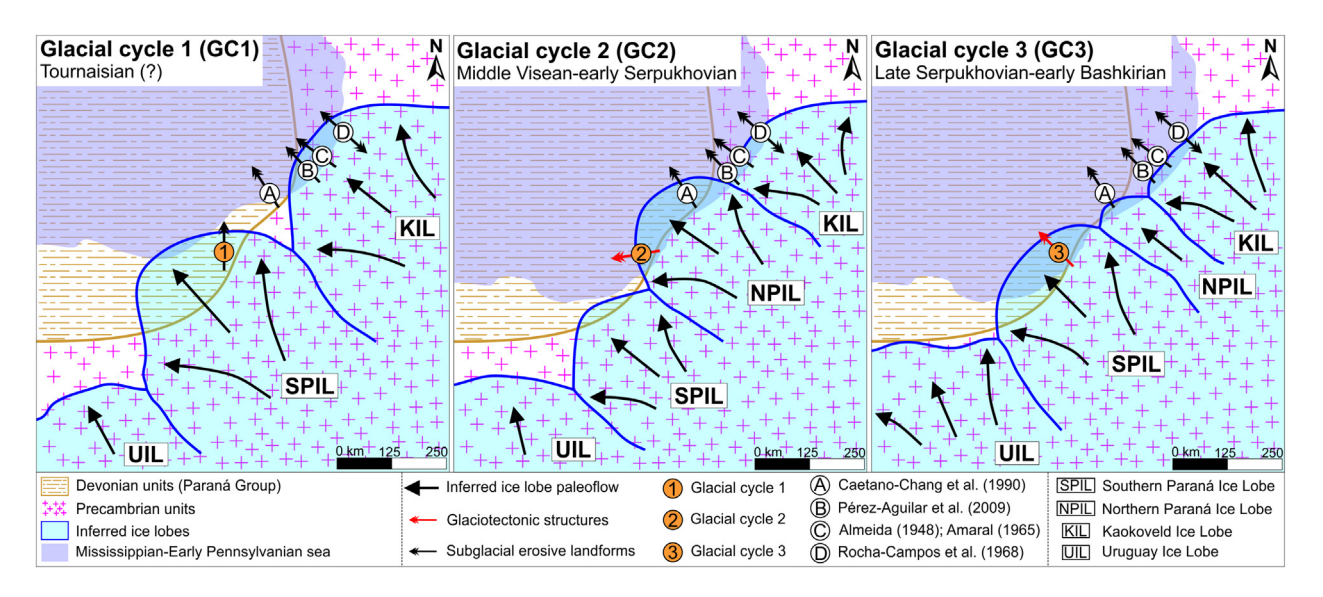


Fig. 16. Postulated paleogeographic model for the Mississippian-Early Pennsylvanian at eastern margin of the Paraná Basin according to the three discussed glacial cycles. Paleogeographic map location shown in reconstructed South America and Africa during Gondwana times in Fig. 15B. Areal distribution of Devonian units obtained from isopach map in Milani and Ramos (1998). Epicontinental sea based on isopach maps of Lagoa Azul Formation from Santos (1987) and França and Potter (1988).

With a similar evolutional history as the WIS, a possible separate ice sheet (Uruguay Ice Sheet; UIS) could be placed over southeastern South America and southwesternmost Africa during the LPIA early stages (Fig. 15B). During the Mississippian, this region was uplifted due to Chañic phase of Gondwanides orogeny (López-Gamundí and Rossello, 1993; Milani and de Wit, 2008), possibly elevating the land surface above the equilibrium line altitude and leading to glacier development. The UIS may be related to the younger Uruguay Ice Lobe (Crowell and Frakes, 1975; Fedorchuk et al., 2018), responsible for generating subglacial features with a north/northwest trend during the Late Pennsylvanian-earliest Permian (Tomazelli and Soliani, 1982, 1997; Assine et al., 2018). Deposition in southernmost Paraná Basin and southwesternmost Africa started during the Late Pennsylvanian (Stollhofen et al., 2008; Griffis et al., 2018a) as accommodation space increased, probably due to UIS waning and sea-level rise.

The Balsa Nova ice-contact complex consists in a rare glaciogenic record of the early stages of the LPIA and brings new insights on the extent of ice cover on Gondwana. It shows that ice sheets covered polar regions of Gondwana while topographically-controlled small ice centers took place at mid-latitudes (e.g., Caputo et al., 2008; Isbell et al., 2012). It also supports the ideas presented by González-Bonorino and Eyles (1995) and Chen et al. (2016), which assume that the maximum ice cover on Gondwana during the LPIA took place at the Mississippian/Pennsylvanian boundary.

10. Conclusions

By combining sedimentology, structural analysis and palynology of an ice-contact complex in the lowermost Itararé Group (Balsa Nova region, eastern Paraná Basin), some conclusions can be drawn concerning LPIA glaciodynamics and paleogeography in this region of west-central Gondwana:

- (1) Three facies association corresponding to subglacial tillites, proximal grounding-line fan deposits, and distal grounding-line fan deposits are recurrent in four defined, informal stratigraphic units at the base of the Lagoa Azul Formation. Such facies association were deformed in subglacial and ice-marginal settings, giving rise to subglacial tillite sheets and push moraine complexes.
- (2) The vertical recurrence of facies association and glaciotectonized intervals record an ice advance/retreat cyclicity designated as GC1, GC2, and GC3. Each glacial cycle corresponds to an ice lobe advance derived from the Windhoek Ice Sheet towards the north, west/southwest and northwest, respectively.
- (3) Subglacial tillites in the lowermost portion of the complex are still unknown if attributed to a continental or a marine glacier. The rest of the ice-contact complex was generated under the influence of advancing and retreating, grounded, temperate ice lobes with tidewater termini in a marine environment. This interpretation contradicts previous interpretations that hypothesize a glaciocontinental (glaciolacustrine) origin for these deposits.
- (4) A previously unpublished middle Visean-early Serpukhovian palynomorph assemblage records the oldest record of the LPIA in Paraná Basin and allows new constraints on the depositional age for the Lagoa Azul Formation in the middle Visean-Moscovian/ Kasimovian boundary. Palynomorphs restricted to the Tournaisian stage are treated as reworked from possibly Tournaisian strata.
- (5) The timing of the three glacial cycles described herein can be correlated to major LPIA glacial episodes defined in other basins of Gondwana: glacial cycle 1 (possibly Tournaisian); glacial cycle 2 (middle Visean-early Serpukhovian); and glacial cycle 3 (late Serpukhovian-early Bashkirian).
- (6) The paleogeographic reconstruction for the Mississippian-Early Pennsylvanian interval within the eastern and southern Paraná Basin, as well as in contiguous regions in Africa, elucidates an earlier growth of ice sheets than classically assumed for the LPIA.

Acknowledgements

This contribution is part of MSc research performed by the first author in the Postgraduate Program in Geology at Universidade Federal do Paraná (UFPR), with scholarship provided by Coordenação de Aperfeiçoamento de Pessoal de Nível Superior (CAPES). We thank all colleagues that collaborated as field assistants, and the Conselho Nacional de Desenvolvimento Científico e Tecnológico (CNPq) for financial support to F. F. Vesely and P. A. de Souza (grants 461650/2014-2, 310727/2014-6, 461628/2014-7). F. F. Vesely and P. A. Souza are research fellows of the CNPq. Support for J.L. Isbell and N.D. Fedorchuk was provided by grants from the USA National Science Foundation (Grants 1443557, 1559231, and 1729219), the University of Wisconsin-Milwaukee Center for Latin American and Caribbean studies, and the Wisconsin Geological Society.

Appendix A. Supplementary data

Supplementary data associated with this article can be found in the online version, at https://doi.org/10.1016/j.sedgeo.2019.03.001. These data include the Google map of the most important areas described in this article.

References

- Aber, J.S., Croot, D.G., Fenton, M.M., 1989. Glaciotectonic Landforms and Structures. Kluwer Academic Publishers, Dordrecht.
- Almeida, F.F.M., 1948. A "Roche Moutonnée" de Salto, Estado de São Paulo. Boletim Geologia e Metalurgia 5, 112–118.
- Alsop, G.I., Marco, S., Levi, T., Weinberger, R., 2017. Fold and thrust systems in mass transport deposits. Journal of Structural Geology 94, 98–115.
- Amaral, S.E., 1965. Nova ocorrência de rocha moutonnée em Salto, SP. Boletim da Sociedade Brasileira de Geologia 14, 71–82.
- Aquino, C.D., Valdez, B.V., V.V., Faccini, U.F., Milana, J.P., Paim, P.S.G., 2016. Facies and depositional architecture according to a jet efflux model of a late Paleozoic tidewater grounding-line system from the Itararé Group (Paraná Basin), southern Brazil. Journal of South American Earth Sciences 67, 180–200.
- Ashley, G.A., Boothroyd, J.C., Borns, H.W., 1991. Sedimentology of late Pleistocene (Laurentide) deglacial-phase deposits, eastern Maine; an example of a temperate marine grounded ice-sheet margin. In: Anderson, J.B., Ashley, G.M. (Eds.), Glacial Marine Sedimentation; Palaeoclimatic Significance. Geological Society of America Special Paper vol. 261, pp. 107–125.
- Assine, M.L., de Santa Ana, H., Veroslavsky, G., Vesely, F.F., 2018. Exhumed subglacial landscape in Uruguay: erosional landforms, depositional environments, and paleo-ice flow in the context of the late Paleozoic Gondwanan glaciation. Sedimentary Geology 369, 1–12
- Benn, D.I., Evans, D.J.A., 2010. Glaciers and Glaciation. Hodder Education, London.
- Bennett, M., Glasser, N., 2009. Glacial Geology: Ice Sheets and Landforms. Wiley-Blackwell, Oxford.
- Bennett, M.R., 2001. The morphology, structural evolution and significance of push moraines. Earth-Science Reviews 53, 197–236.
- Berthelsen, A., 1978. The methodology of kineto-stratigraphy as applied to glacial geology. Bulletin of the Geological Society of Denmark 27, 25–38.
- Bigarella, J.J., Salamuni, R., Fuck, R.A., 1967. Striated surfaces and related features, developed by the Gondwana ice sheets (state of Parana, Brazil). Palaeogeography, Palaeoclimatology, Palaeoecology 3, 265–276.
- Boulton, G.S., 1990. Sedimentary and sea level changes during glacial cycles and their control on glaciomarine facies architecture. In: Dowdeswell, J.A., Scourse, J.D. (Eds.), Glacimarine Environments: Processes and Sediments. Geological Society, London, Special Publications vol. 53, pp. 15–52.
- Boulton, G.S., 1996. Theory of glacial erosion, transport and deposition as a consequence of subglacial sediment deformation. Journal of Glaciology 42, 43–62.
- Boulton, G.S., Deynoux, M., 1981. Sedimentation in glacial environments and the identification of tills and tillites in ancient sedimentary sequences. Precambrian Research 15, 397–422
- Boulton, G.S., van der Meer, J.J.M., Beets, D.J., Hart, J.K., Ruegg, G.H.J., 1999. The sedimentary and structural evolution of a recent push moraines complex: Holmstrømbreen, Spitsbergen. Quaternary Science Reviews 18, 339–371.
- Brauer, A., 2004. Annually laminated lake sediments and their palaeoclimatic relevance. In: Fischer, H., Kumke, T., Lohmann, G., Flöser, G., Miller, H., von Storch, H., Negendank, J.F.W. (Eds.), The Climate in Historical Times. Springer-Verlag, Berlin, pp. 109–128.
- Bussert, R., 2010. Exhumed erosional landforms of the Late Palaeozoic glaciation in northern Ethiopia: indicators of ice-flow direction, palaeolandscape and regional ice dynamics. Gondwana Research 18, 356–369.
- Caetano-Chang, M.R., 1984. Análise Ambiental e Estratigráfica do Subgrupo Itararé (PC) no Sudoeste do Estado de São Paulo. Universidade de São Paulo, São Paulo (PhD Thesis).
- Caetano-Chang, M.R., Oliveira, J.P., Brighetti, J.M.P., 1990. Pavimento estriado em rochas do Subgrupo Itararé ao longo do Rio Piritubinha, sul do estado de São Paulo. Revista Brasileira de Geociencias 20, 333–335.

- Cagliari, J., Philipp, R.P., Valdez, B.V., Netto, R.G., Hillebrand, P.K., Lopes, R.C., Basei, M.A.S., Faccini, U.F., 2016. Age constraints of the glaciation in the Paraná Basin: evidence from new U-Pb dates. Journal of the Geological Society 173, 871–874.
- Canuto, J.R., Santos, P.R., Rocha-Campos, A.C., 2010. Fácies e associações de fácies de diamictitos do Subgrupo Itararé (Paleozóico Superior) no norte de Santa Catarina e sul do Paraná. Bacia do Paraná. Brasil. Revista Brasileira de Geociencias 40. 220–235.
- Caputo, M.V., Melo, J.H.G., Streel, M., Isbell, J.L., 2008. Late Devonian and early Carboniferous glacial records of South America. In: Fielding, C.R., Frank, T.D., Isbell, J.L. (Eds.), Resolving the Late Paleozoic Ice Age in Time and Space. Geological Society of America Special Paper vol. 441, pp. 161–173.
- Carvalho, A.H., Vesely, F.F., 2016. Facies relationships recorded in a Late Paleozoic fluviodeltaic system (Paraná Basin, Brazil): insights into the timing and triggers of subaqueous sediment gravity flows. Sedimentary Geology 352, 45–62.
- Castro, L.G., Ferreira, F.J.F., Cury, L.F., Fiori, A.P., Soares, P.C., Lopes, A.P., Oliveira, M.J., 2014. Interpretação qualitativa e semiquantitativa dos dados aeromagnéticos sobre a Zona de Cisalhamento Lancinha, porção meridional do Cinturão Ribeira no Estado do Paraná, Sul do Brasil. Geologia USP Série Científica 14, 3–18.
- Césari, S.N., Gutiérrez, P.R., 2000. Palynostratigraphy of upper Paleozoic sequences in central-western Argentina. Palynology 24, 113–146.
- Césari, S.N., Limarino, C.O., Gulbranson, E.L., 2011. An Upper Paleozoic biochronostratigraphic scheme for the western margin of Gondwana. Earth-Science Reviews 106, 149–160.
- Chen, B., Joachimski, M.M., Wang, X., Shen, S., Qi, Y., Qie, W., 2016. Ice volume and paleoclimate history of the late Paleozoic Ice Age from conodont apatite oxygen isotopes from Naqing (Guizhou, China). Palaeogeography, Palaeoclimatology, Palaeoecology 448, 151–161
- Clayton, G., Loboziak, S., Streel, M., Turnau, E., Utting, J., 1990. Palynological events in the Mississipian (lower Carboniferous) of Europe, North Africa and North America. Courier Forschungsistitut Senckenberg 130, 79–84.
- Colgan, P.M., Mickelson, D.M., 1997. Genesis of streamlined landforms and flow history of the Green Bay Lobe, Wisconsin, USA. Sedimentary Geology 111, 7–25.
- Croot, D.G., 1987. Glacio-tectonic structures: a mesoscale model of thin-skinned thrust sheets? Journal of Structural Geology 9, 797–808.
- Crowell, J.C., 1999. Pre-Mesozoic Ice Ages: Their Bearing on Understanding the Climate System. Geological Society of America, Memoir 192. The Geological Society of America, Boulder.
- Crowell, J.C., Frakes, L.A., 1975. The late Paleozoic Glaciation. In: Campbell, K.S.W. (Ed.), Gondwana Geology. Papers presented at the Third Gondwana Symposium. Australian National University Press, Canberra, pp. 313–331.
- Daemon, R.F., Quadros, L.P., 1970. Bioestratigrafia do Neopaleozóico da Bacia do Paraná. Anais do 24° Congresso Brasileiro de Geologia. Sociedade Brasileira de Geologia, Brasília, pp. 359–412.
- van der Meer, J.J.M., Menzies, J., Rose, J., 2003. Subglacial till: the deforming glacier bed. Quaternary Science Reviews 22, 1659–1685.
- van der Wateren, F.M., 1985. A model of glacial tectonics, applied to the ice-pushed ridges in Central Netherlands. Bulletin of the Geological Society of Denmark 34, 55–74.
- van der Wateren, F.M., 1994. Proglacial subaquatic outwash fan and delta sediments in push moraines – indicators of subglacial meltwater activity. Sedimentary Geology 91, 145–172.
- van der Wateren, F.M., 1995. Structural geology and sedimentology of Push Moraines: processes of soft sediment deformation in a glacial environment and the distribution of glaciotectonic styles. Mededelingen Rijks Geologische Dienst 54, 1–168.
- van der Wateren, F.M., 2002. Processes of glaciotectonism. In: Menzies, J. (Ed.), Modern and Past Glacial Environments. Butterworth Heinemann, Oxford, pp. 417–444.
- van der Wateren, F.M., Kluiving, S.J., Bartek, L.R., 2000. Kinematic indicators of subglacial shearing. In: Maltman, A.J., Hubbard, B., Hambrey, M.J. (Eds.), Deformation of Glacial Materiais. Geological Society, London, Special Publications vol. 176, pp. 259–278.
- Dowdeswell, J.A., Hogan, K.A., Arnold, N.S., Mugford, R.I., Wells, M., Hirst, J.P.P., Decalf, C., 2015. Sediment-rich meltwater plumes and ice-proximal fans at the margins of modern and ancient tidewater glaciers: observations and modelling. Sedimentology 62, 1665–1692.
- Dykstra, M., Garyfalou, K., Kertznus, V., Kneller, B., Milana, J.P., Molinaro, M., Szuman, M., Thompson, P., 2011. Mass-transport deposits: combining outcrop studies and seismic forward modeling to understand lithofacies distributions, deformation, and their seismic stratigraphic expression. In: Shipp, R.C., Weimer, P., Posamentier, H.W. (Eds.), Mass-Transport Deposits in Deepwater Settings. SEPM Special Publication vol. 96, pp. 293–310.
- Evans, D.J.A., Phillips, E.R., Hiemstra, J.F., Auton, C.A., 2006. Subglacial till: formation, sedimentary characteristics and classification. Earth-Science Reviews 78, 115–176.
- Eyles, C.H., Eyles, N., Miall, A.D., 1985. Models of glaciomarine sedimentation and their application to the interpretation of ancient glacial sequences. Palaeogeography, Palaeoclimatology, Palaeoecology 51, 15–84.
- Eyles, N., Eyles, C.H., Woodworth-Lynas, C.M.T., Randall, T.A., 2005. The sedimentary record of drifting ice (early Wisconsin Sunybrook deposit) in an ancestral icedammed Lake Ontario, Canada. Quaternary Research 63, 171–181.
- Fallgatter, C., Paim, P.S.G., 2017. On the origin of the Itararé Group basal nonconformity and its implications for the Late Paleozoic glaciation in the Paraná Basin, Brazil. Palaeogeography, Palaeoclimatology, Palaeoecology https://doi.org/10.1016/j. palaeo.2017.02.039 (in press).
- Fedorchuk, N.D., Isbell, J.L., Griffis, N.P., Montañez, I.P., Vesely, F.F., Iannuzzi, R., Mundil, R., Yin, Q., Pauls, K.N., Rosa, E.L.M., 2018. Origin of paleovalleys on the Rio Grande do Sul shield (Brazil): implications for the extent of late Paleozoic glaciation in west-central Gondwana. Palaeogeography, Palaeoclimatology, Palaeoecology https://doi.org/ 10.1016/j.palaeo.2018.04.013 (in press).
- Fielding, C.R., Frank, T.D., Isbell, J.L., 2008. The late Paleozoic ice age a review of current understanding and synthesis of global climate patterns. In: Fielding, C.R., Frank, T.D.,

- Isbell, J.L. (Eds.), Resolving the Late Paleozoic Ice Age in Time and Space. Geological Society of America, Special Paper vol. 441, pp. 343–354.
- Fitzsimons, S., Howarth, J., 2018. Glaciolacustrine processes. In: Menzies, J., van der Meer, J. (Eds.), Past Glacial Environments. Elsevier, Amsterdan, pp. 309–334.
- Frakes, L.A., 1979. Climates throughout Geologic Time. Elsevier, Amsterdan.
- França, A.B., Potter, P.E., 1988. Estratigrafia, ambiente deposicional e análise de reservatório do Grupo Itararé (Permocarbonífero), Bacia do Paraná (parte 1). Boletim de Geociências da Petrobrás 2. 147–191.
- Fuck, R.A., 1966. Nota explicativa da folha geológica de Quero-Quero. Boletim da Universidade Federal do Paraná, Geologia 19, 1–21.
- Fúlfaro, V.J., 1996. Geología del Paraguay Oriental. In: Comin-Chiaramonti, P., Gomes, C.B. (Eds.), Magmatismo alcalino en Paraguay Central-Oriental: relaciones con magmatismo coeval en Brasil. Edusp/Fapesp, São Paulo, pp. 17–29.
- González-Bonorino, G., Eyles, N., 1995. Inverse relation between ice extent and the late Paleozoic glacial record of Gondwana. Geology 23, 1015–1018.
- Griffis, N.P., Mundil, R., Montañez, I.P., Isbell, J., Fedorchuk, N., Vesely, F.F., Iannuzzi, R., Yin, Q.Z., 2018a. A new stratigraphic framework built on U-Pb single-zircon TIMS ages and implications for the timing of the penultimate icehouse (Paraná Basin, Brazil). Geological Society of America Bulletin 130, 848–858.
- Griffis, N.P., Montañez, I.P., Fedorchuck, N., Isbell, J., Mundil, R., Vesely, F., Weinshultz, L., Iannuzzi, R., Gulbanson, R., Taboada, A., Pagani, A., Sanborn, M.E., Huyskens, M., Wimpenny, J., Linol, B., Yin, Q.Z., 2018b. Isotopes to ice: constraining provenance of glacial deposits and ice centers in west-central Gondwana. Palaeogeography, Palaeoclimatology, Palaeoecology https://doi.org/10.1016/j.palaeo.2018.04.020 (in press).
- Hambrey, M.J., Glasser, N.F., 2012. Discriminating glacier thermal and dynamic regimes in the sedimentary record. Sedimentary Geology 251-252, 1–33.
- Hart, J.K., 1995. Subglacial erosion, deposition and deformation associated with deformable beds. Progress in Physical Geography 19, 173–191.
- Hart, J.K., Boulton, G.S., 1991. The interrelation of glaciotectonic and glaciodepositional processes within the glacial environment. Quaternary Science Reviews 10, 335–350.
- Hart, J.K., Roberts, D.H., 1994. Criteria to distinguish between subglacial glaciotectonic and glaciomarine sedimentation, I. Deformation styles and sedimentology. Sedimentary Geology 91, 191–213.
- Hart, J.K., Watts, R.J., 1997. A comparison of the styles of deformation associated with two recent push moraines, South Van Keulenfjorden, Svalbard. Earth Surface Processes and Landforms 22, 1089–1107.
- Hart, J.K., Hindmarsh, R.C.A., Boulton, G.S., 1990. Styles of subglacial glaciotectonic deformation within the context of the Anglian Ice-sheet. Earth Surface Processes and Landforms 15, 227–241.
- Henry, L.C., Isbell, J.L., Limarino, C.O., 2008. Carboniferous glacigenic deposits of the proto-Precordillera of west-central Argentina. In: Fielding, C.R., Frank, T.D., Isbell, J.L. (Eds.), Resolving the Late Paleozoic Ice Age in Time and Space. Geological Society of America Special Paper vol. 441, pp. 131–142.
- Henry, L.C., Isbell, J.L., Fielding, C.R., Domack, E.W., Frank, T.D., Fraiser, M.L., 2012. Proglacial deposition and deformation in the Upper Carboniferous to lower Permian Wynyard Formation, Tasmania: a process analysis. Palaeogeography, Palaeoclimatology, Palaeoecology 315-316, 142–157.
- Higgs, K.T., 1990. Upper Viséan and lower Namurian miospore assemblages from County Cork, Ireland. Irish Journal of Earth Sciences 10, 115–127.
- Holz, M., França, A.B., Souza, P.A., Iannuzzi, R., Rohn, R., 2010. A stratigraphic chart of the late Carboniferous/Permian succession of the eastern border of the Paraná Basin, Brazil, South America. Journal of South American Earth Sciences 29, 381–399.
- Ingólfsson, O., 1987. The Late Wichselian glacial geology of the Melabakkar-Ásbakkar coastal cliffs, Borgarfördur, W-Iceland. Jökull 37, 57–80.
- Isbell, J.L., 2010. Environmental and paleogeographic implications of glaciotectonic deformation of glaciomarine deposits within Permian strata of the Metschel Tillite, southern Victoria Land, Antarctica. In: López-Gamundí, O.R., Buatois, L.A. (Eds.), Late Paleozoic Glacial Events and Postglacial Transgressions in Gondwana. Geological Society of America Special Paper vol. 468, pp. 81–100.
- Isbell, J.L., Miller, M.F., Wolfe, K.L., Lenaker, P.A., 2003. Timing of Paleozoic glaciation in Gondwana: was glaciation responsible for the development of northern hemisphere cyclothems? In: Chan, M.A., Archer, A.W. (Eds.), Extreme Depositional Environments: Mega End Members in Geologic Time. Geological Society of America Special Paper vol. 370, pp. 5–24
- Isbell, J.L., Henry, L.C., Gulbranson, E.L., Limarino, C.O., Fraiser, M.L., Koch, Z.J., Ciccioli, P.L., Dineen, A.A., 2012. Glacial paradoxes during the late Paleozoic ice age: evaluating the equilibrium line altitude as control on glaciation. Gondwana Research 22, 1–19.
- Kehew, A.E., Esch, J.M., Kozlowski, A.L., Ewald, S.K., 2012. Glacial landsystems and dynamics of the Saginaw Lobe of the Laurentide Ice Sheet, Michigan, USA. Quaternary International 260, 21–31.
- Kipper, F., Souza, P.A., Vesely, F.F., 2017. Palinomorfos e associações de fácies da Formação Lagoa Azul (Grupo Itararé, Pennsilvaniano da Bacia do Paraná) no sudeste do Estado do Paraná, Brasil. Pesquisa em Geociências 44, 93–108.
- Kluiving, S.J., 1994. Glaciotectonics of the Itterbeck Uelsen push moraines, Germany. Journal of Ouaternary Science 9, 235–244.
- Lawver, L.A., Dalziel, I.W.D., Norton, I.O., Gahagan, L.M., 2011. The Plates 2011 Atlas of Plate Reconstructions (500 Ma to Present Day). Plates Progress Report No. 345-0811, University of Texas Technical Report No. 198. University of Texas, Austin.
- Le Heron, D.P., 2017. An exhumed Paleozoic glacial landscape in Chad. Geology 46, 91–94.
- Limarino, C.O., Césari, S.N., Spaletti, L.A., Taboada, A.C., Isbell, J.L., Geuna, S., Gulbranson, E.L., 2014. A paleoclimatic review of southern South America during the late Paleozoic: a record from icehouse to extreme greenhouse conditions. Gondwana Research 25, 1396–1421.

- López-Gamundí, O.R., Rossello, E.A., 1993. Devonian-Carboniferous unconformity in Argentina and its relation to the Eo-Hercynian orogeny in southern South America. Geologische Rundschau 82. 136–147.
- Martin, H., 1961. The Hypothesis of Continental Drift in the Light of Recent Advances of Geological Knowledge in Brazil and in South West Africa. Alex L. du Toit Memorial Lectures 7. The Geological Society of South Africa
- Martin, H., 1981. The Late Palaeozoic Dwyka Group of the South Kalahari Basin in Namibia and Botswana and the subglacial valleys of the Kaokoveld in Namibia. In: Hambrey, M.J., Harland, W.B. (Eds.), Earth's Pre-Pleistocene Glacial Record. Cambridge University Press. Cambridge. pp. 61–66.
- Martinsen, O., 1994. Mass movements. In: Maltman, A. (Ed.), The Geological Deformation of Sediments. Chapman & Hall, London, pp. 127–165.
- McCabe, A.M., Eyles, N., 1988. Sedimentology of an ice-contact glaciomarine delta, Carey Valley, Northern Ireland. Sedimentary Geology 59, 1–14.
- McCarroll, D., Rijsdijk, K.F., 2003. Deformation styles as a key for interpreting glacial deposition environments. Journal of Quaternary Science 18, 473–489.
- Melo, J.H.G., Loboziak, S., 2003. Devonian-Early Carboniferous miospore biostratigraphy of the Amazon Basin, Northern Brazil. Review of Paleobotany and Palynology 124, 131–202
- Melo, J.H.G., Playford, G., 2012. Miospore Palynology and Biostratigraphy of Mississippian Strata of the Amazonas Basin, Northern Brazil. Part Two. AASP, Contribution Series 47 pp. 91–201.
- Menzies, J., van der Meer, J.J.M., Shilts, W.W., 2018. Subglacial processes and landforms. In: Menzies, J., van der Meer, J. (Eds.), Past Glacial Environments. Elsevier, Amsterdan, pp. 105–158.
- Milani, E.J., de Wit, M.J., 2008. Correlations between the classic Paraná and Cape-Karoo sequences of South America and southern Africa and their basin infills flaking the Gondwanides: du Toit revisited. In: Pankhurst, R.J., Trouw, R.A.J., Brito Neves, B.B., de Wit, M.J. (Eds.), West Gondwana: Pre-Cenozoic Correlations across the South Atlantic Region. Geological Society, London, Special Publications vol. 294, pp. 319–342.
- Milani, E.J., Ramos, V.A., 1998. Orogenias paleozoicas no domínio sul-ocidental do Gondwana e os ciclos de subsidência na Bacia do Paraná. Revista Brasileira de Geociencias 28, 473–484.
- Molnia, B.F., 1989. Subartic (Temperate) Glacial-Marine sedimentation, The Northeast Gulf of Alaska. In: Anderson, J.B., Molnia, B.F. (Eds.), Glacial-Marine Sedimentation. 28th International Geological Congress, Washington, Short Course 9, pp. 59–106.
- Mottin, T.E., Vesely, F.F., Rodrigues, M.C.N.L., Kipper, F., Souza, P.A., 2018. The paths and timing of late Paleozoic ice revisited: new stratigraphic and paleo-ice flow interpretations from a glacial succession in the upper Itararé Group (Paraná Basin, Brazil). Palaeogeography, Palaeoclimatology, Palaeoecology 490, 488–504.
- Mulder, T., Alexander, J., 2001. The physical character of subaqueous sedimentary density flows and their deposits. Sedimentology 48, 269–299.
- Muratori, A., 1966. Nota explicativa da folha geológica de Campo Largo. Boletim da Universidade Federal do Paraná, Geologia 21.
- Murray, T., 1994. Glacial deformation. In: Maltman, A. (Ed.), The Geological Deformation of Sediments. Chapman & Hall, London, pp. 73–93.
- Owens, B., McLean, D., Bodman, D., 2004. A revisted palyzonation of British Namurian deposits and comparisons with eastern Europe. Micropaleontology 50, 89–103.
- di Pasquo, M., 2007a. Associaciones palinológicas en las formaciones Los Monos (Devónico) e Itacua (Carbonífero Inferior) en Balapuca (Cuenca Tarija), sur de Bolivia. Parte 1. Formación los monos. Revista Geológica de Chile 34, 97–137.
- di Pasquo, M., 2007b. Associaciones palinológicas en las formaciones Los Monos (Devónico) e Itacua (Carbonífero Inferior) en Balapuca (Cuenca Tarija), sur de Bolivia. Parte 2. Associaciones de la Formacion Itacua e interpretación estratigráfica y cronologia de las formaciones Los Monos e Itacua. Revista Geológica de Chile 34, 163–198.
- Pérez Loinaze, V., 2007. A Mississippian miospore biozone for southern Gondwana. Palynology 31, 101–117.
- Pérez Loinaze, V., 2008a. Systematic palynological study of the Cortaderas Formation, (Mississipian) Río Blanco Basin, Argentina. Part One. Ameghiniana 45, 33–57.
- Pérez Loinaze, V., 2008b. Systematic palynological study of the Cortaderas Formation, (Mississipian) Río Blanco Basin, Argentina. Part Two. Ameghiniana 45, 421–441.
- Pérez Loinaze, V., Limarino, C.O., Césari, S.N., 2010. Glacial events in Carboniferous sequences from Paganzo and Río Blanco basins (Northwest Argentina): Palynology and depositional setting. Geologica Acta 8, 339–418.
- Pérez-Aguilar, A., Petri, S., Hypólito, R., Ezaki, S., Souza, P.A., Juliani, C., Monteiro, L.V.S., Moschini, F.A., 2009. Superfícies estriadas no embasamento granítico e vestígio de pavimento de clastos neopaleozoicos na região de Salto, SP. Revista Escola de Minas 62, 17–22.
- Phillips, E.R., 2018. Glacitectonics. In: Menzies, J., van der Meer, J. (Eds.), Past Glacial Environments. Elsevier, Amsterdam, pp. 467–502.
- Playford, G., 2015. Mississippian palynoflora from the northern Perth Basin, Western Australia: systematics and stratigraphical and palaeogeographical significance. Journal of Systematic Palynology 14, 731–770.
- Playford, G., Melo, J.H.G., 2012. Miospore Palynology and Biostratigraphy of Mississippian Strata of the Amazonas Basin, Northern Brazil. Part One. AASP, Contribution Series 47 pp. 1–89.
- Playford, G., Mory, A.J., 2017. Composition and occurrence of the Grandispora maculosa zonal assemblage (Mississippian) in the subsurface of the Carnavon basin and the Coolcalalaya sub-basin of western Australia, and its Gondwanan distribution. Revista Italiana di Paleontologia e Stratigrafia 123, 275–318.
- Powell, R.D., 1990. Glacimarine processes at grounding-line fans and their growth to icecontact deltas. In: Dowdeswell, J.A., Scourse, J.D. (Eds.), Glacimarine Environments: Processes and Sediments. Geological Society Special Publication vol. 53, pp. 53–73.
- Powell, R.D., 1994. Glacimarine processes and inductive lithofacies modelling of ice shelf and tidewater glacier sediments based on Quaternary examples. Marine Geology 57, 1–52.

- Powell, R.D., Alley, R.B., 1997. Grounding-line systems: processes, glaciological inferences and the stratigraphic record. In: Barker, P.F., Cooper, A.K. (Eds.), Geology and Seismic Stratigraphy of the Antarctic Margin. Antarctic Research Series 71. American Geophysical Union, pp. 169–187.
- Powell, R.D., Domack, E., 2002. Modern glaciomarine environments. In: Menzies, J. (Ed.), Modern and Past Glacial Environments. Butterworth Heinemann, Oxford, pp. 361–390.
- Powell, R.D., Molnia, B.F., 1989. Glacimarine sedimentary processes, facies and morphology of the south-Southeast Alaska Shelf and fjords. Marine Geology 85, 359–390.
- Puigdomenech, C.G., Carvalho, B., Paim, P.S.G., Faccini, U.F., 2014. Lowstand turbidites and delta systems of the Itararé Group in the Vidal Ramos region (SC), southern Brazil. Brazilian Journal of Geology 44, 529–544.
- Richardson, J.C., 2008. Rare palynomorphs from the Nancy Member of the Borden Formation (Mississippian; Tournaisian), Kentucky, U.S.A. Northeastern Geology and Environmental Sciences 30, 295–303.
- Rijsdijk, K.F., Owen, G., Warren, W.P., McCaroll, D., van der Meer, J.J.M., 1999. Clastic dykes in over-consolidated tills: evidence for subglacial hydrofracturing at Killiney Bay, eastern Ireland. Sedimentary Geology 129, 111–126.
- Rijsdijk, K.F., Warren, W.P., van der Meer, J.J.M., 2010. The glacial sequence at Killiney, SE Ireland: terrestrial deglaciation and polyphase glacitectonic deformation. Quaternary Science Reviews 29, 696–719.
- Rocha-Campos, A.C., Santos, P.R., 1981. The Itararé Subgroup, Aquidauana Group and San Gregório Formation, Paraná Basin, southeastern South America. In: Hambrey, M.J., Harland, W.B. (Eds.), Earth's Pre-Pleistocene Glacial Record. Cambridge University Press, Cambridge, pp. 842–852.
- Rocha-Campos, A.C., Farjallat, J.E., Yoshida, R., 1968. New glacial features of the Upper Paleozoic Itararé Subgroup in the State of São Paulo, Brazil. Boletim da Sociedade Brasileira de Geologia 17. 47–57.
- Rocha-Campos, A.C., Canuto, J.R., Santos, P.R., 2000. Late Paleozoic glaciotectonic structures in northern Paraná Basin, Brazil. Sedimentary Geology 130, 131–143.
- Rocha-Campos, A.C., Basei, M.A.S., Nutman, A.P., Santos, P.R., 2006. SHRIMP U-Pb zircon geochronological calibration of the late Paleozoic supersequence, Paraná Basil, Brazil. Abstracts of the 5th South American Symposium on Isotope Geology. Punta del Este, pp. 298–301.
- Rocha-Campos, A.C., Basei, M.A.S., Nutman, A.P., Santos, P.R., Passarelli, C.R., Caline, F.M., Rosa, O.C.R., Fernandes, M.T., Santa Ana, H., Veroslavsky, G., 2019. U-Pb zircon dating of ash fall deposits from the Paleozoic Paraná Basin of Brazil and Uruguay: a reevaluation of the stratigraphic correlations. The Journal of Geology 127, 167–182.
- Rosa, E.L.M., Vesely, F.F., França, A.B., 2016. A review on late Paleozoic ice-related landforms in the Paraná Basin: origin and paleogeographical implications. Brazilian Journal of Geology 46, 147–166.
- Russell, H.A.J., Arnott, R.W.C., 2003. Hydraulic-jump and hyperconcentrated-flow deposits of a glacigenic subaqueous fan: Oak Ridge moraine, southern Ontario, Canada. Journal of Sedimentary Research 73, 887–905.
- Santos, P.R., 1987. Fácies e Evolução Paleogeográfica do Subgrupo Itararé/Grupo Aquidauana (Neopaleozóico) na Bacia do Paraná, Brasil. Universidade de São Paulo, São Paulo (PhD Thesis).
- Santos, P.R., Rocha-Campos, A.C., Canuto, J.R., 1996. Patterns of late Paleozoic deglaciation in the Parana Basin, Brazil. Palaeogeography, Palaeoclimatology, Palaeoecology 125, 165–184.
- Sobiesiak, M.S., Alsop, G.I., Kneller, B., Milana, J.P., 2017. Sub-seismic scale folding and thrusting within an exposed mass transport deposit: a case study from NW Argentina. Journal of Structural Geology 96, 176–191.
- Sobiesiak, M.S., Kneller, B., Alsop, G.I., Milana, J.P., 2018. Styles of basal interaction beneath mass transport deposits. Marine and Petroleum Geology 98, 629–639.
- Souza, P.A., 2006. Late Carboniferous palynostratigraphy of the Itararé Subgroup, northeastern Paraná Basin, Brazil. Review of Palaeobotany and Palynology 138, 9–29.
- Starck, D., Gallardo, E., Schulz, A., 1993. The pre-Carboniferous unconformity in the Argentine portion of the Tarija basin. Comptes Rendus of XII International Congress on Carboniferous-Permian 2, Buenos Aires, pp. 373–384.
- Stollhofen, H., Werner, M., Stanistreet, I.G., Armstrong, R.A., 2008. Single-zircon U-Pb dating of Carboniferous-Permian tuffs, Namibia, and the intercontinental deglaciation cycle framework. In: Fielding, C.R., Frank, T.D., Isbell, J.L. (Eds.), Resolving the Late Paleozoic Ice Age in Time and Space. Geological Society of America Special Paper vol. 441, pp. 83–96.
- Stow, D.A., Shanmugam, G., 1980. Sequence of structures in fine-grained turbidites: comparison of recent deep-sea and ancient flysch sediments. Sedimentary Geology 25, 23–42.
- Strugale, M., Rostirolla, S.P., Mancini, F., Portela Filho, C.V., Ferreira, F.J.F., Freitas, R.C., 2007. Structural framework and Mesozoic-Cenozoic evolution of Ponta Grossa Arch, Paraná Basin, southern Brazil. Journal of South American Earth Sciences 24, 203–227.
- Tomazelli, L.J., Soliani, E., 1982. Evidências de atividade glacial no Paleozoico Superior do Rio Grande do Sul. Anais do 32° Congresso Brasileiro de Geologia 4. Sociedade Brasileira de Geologia, Salvador, pp. 1378–1391.
- Tomazelli, L.J., Soliani, E., 1997. Sedimentary facies and depositional environments related to Gondwana Glaciation in Batovi and Suspiro Regions, Rio Grande do Sul, Brazil. Journal of South American Earth Sciences 10, 295–303.
- Trosdtorf, I., Assine, M.L., Vesely, F.F., Rocha-Campos, A.C., Santos, P.R., Tomio, A., 2005.
 Glacially striated, soft sediment surfaces on late Paleozoic tillite at São Luiz do Purunã, PR. Anais da Academia Brasileira de Ciências 77. 367–378.
- Valdez, B.V., Aquino, C.D., Paim, P.S.G., Souza, P.A., Mori, A.L., Fallgatter, C., Milana, J.P., Kneller, B., 2017. Late Paleozoic glacial cycles and subcycles in western Gondwana: correlation of surface and subsurface data of the Paraná Basin, Brazil. Palaeogeography, Palaeoclimatology, Palaeoecology https://doi.org/10.1016/j.palaeo.2017.09.004 (in press).

- Vesely, F.F., Assine, M.L., 2006. Deglaciation sequences in the Permo-Carboniferous Itararé Group Paraná Basin, southern Brazil. Journal of South American Earth Sciences 22, 56–168.
- Vesely, F.F., Assine, M.L., 2014. Ice-keel scour marks in the geological record: evidence from carboniferous soft-sediment striated surfaces in the Paraná Basin, southern Brazil. Journal of Sedimentary Research 84. 26–39.
- Vesely, F.F., Trzaskos, B., Kipper, F., Assine, M.L., Souza, P.A., 2015. Sedimentary record of a fluctuating ice margin from the Pennsylvanian of western Gondwana: Paraná Basin, southern Brazil. Sedimentary Geology 326, 45–63.
 Vesely, F.F., Rodrigues, M.C.L.N., Rosa, E.L.M., Amato, J.A., Trzaskos, B., Isbell, J., Fedorchuk,
- Vesely, F.F., Rodrigues, M.C.L.N., Rosa, E.L.M., Amato, J.A., Trzaskos, B., Isbell, J., Fedorchuk, N.D., 2018. Recurrent emplacement of non-glacial diamictite during the late Paleozoic ice age. Geology 46, 615–618.
- Visser, J.N.J., 1987. The Paleogeography of part of Southwestern Gondwana during the Permo-Carboniferous Glaciation. Palaeogeography, Palaeoclimatology, Palaeoecology 61, 205–219.
- Visser, J.N.J., Colliston, W.P., Terblanche, J.C., 1984. The origin of soft-sediment deformation structures in Permo-Carboniferous glacial and proglacial beds, South Africa. Journal of Sedimentary Petrology 54, 1183–1196.
- Walker, R.G., 1965. The origin and significance of the internal sedimentary structures of turbidites. Proceedings of the Yorkshire Geological Society 35, 1–32.

 Woodworth-Lynas, C.M.T., Dowdeswell, J.D., 1994. Soft-sediment striated surfaces and
- Woodworth-Lynas, C.M.T., Dowdeswell, J.D., 1994. Soft-sediment striated surfaces and massive diamicton facies produced by floating ice. In: Deynoux, M., Miller, J.M.J., Domack, E.W., Eyles, N., Fairchild, I.J., Young, G.M. (Eds.), Earth's Glacial Record. Cambridge University Press, Cambridge, pp. 241–259.